# Development and Application of a Global Ocean Wave Prediction Model including Nonlinear Interactions and Dissipation

非線形干渉および消波効果を考慮した
全球波浪モデルの構築と応用

Yasushi SUZUKI

鈴　木　靖

# Development and Application of a Global Ocean Wave Prediction Model including Nonlinear Interactions and Dissipation

Yasushi SUZUKI

## Abstract

Global ocean wave characteristics is investigated by means of an ocean wave hindcast over a long period, using a new ocean wave model.

A new third generation ocean wave model JWA3G is developed in which fundamental physical processes relating to the evolution of the ocean wave field and an original finite difference scheme for the propagation of wave energy are implemented. An improved discrete interaction approximation is developed for the calculation of nonlinear energy transfer due to resonant wave-wave interaction. This new approximation scheme succeeds in improving the accuracy of the approximation of nonlinear energy transfer for sharp spectra. A new formula for the dissipation of wave energy is proposed. It is introduced that the energy dissipation is proportional to $\omega^3$, where $\omega$ is the angular frequency, on the basis of the energy balance in the equilibrium range of the wave spectrum. It is also found that the formula for energy dissipation is independent of the wave height and period, in consideration of the 3/2 power law between wave height and period by Toba (1972). A new Hybrid Upstream scheme, which has the merit of small computational diffusion, is proposed for the calculation of energy propagation and the applicability to the wave model is discussed. The basic characteristics of the model are verified by the SWAMP (1985) experiment and it becomes clear that JWA3G gives valid results which satisfy the 3/2 power law.

The accuracy of the model is verified by comparison with NOAA buoys and GEOSAT data. As a result of this, it is found that the JWA3G has a better accuracy than older wave models in the case of a sudden change of wind field and the decrease of wave height. The total accuracy of wave height for a period of 10 years is found to be 0.7-0.9 m in RMS error and 0.65-0.85 in correlation coefficient. The accuracy of wave period is less than that of wave height. In the north Pacific Ocean, the bias error of wave height is remarkable especially before 1985, while in the north Atlantic Ocean, it is not. The reason is considered to be the lack of accuracy of the wind field and the long life of the swell component of the model. The problem of swell is a weak point of JWA3G for the present and it needs to be improved by considering experimental and theoretical studies on the interaction between swell, and other factors. From the comparison with

GEOSAT data, it is found that the change of wave height in the meridional direction is expressed well by the model, but there is also the problem of a bias error of wave height in the Pacific Ocean.

From considerations of global ocean wave characteristics by means of the wave hindcast results for 10 years, some new ocean wave characteristics, which were never understood from the visually-observed data, become clear. The annual and seasonal variation of the distribution of wave field becomes clear. As a result of swell analysis, the propagation of swell from the Antarctic Sea to the coast of California and the distribution of bi-directional waves are clearly illustrated. The prediction of the bi-directional waves will be an important tool to prevent disasters at sea. The decadal variation of wave height is analyzed, and it is found that the globally averaged wave height was decreasing at a rate of 1.9 cm per year; but the tendency varied between locations. However, the accuracy of the analyzed wind data changed year by year, and a further analysis of the variation of wave height is needed in relation to climate change.

The development of a new third generation wave model with a highly accurate scheme will be useful not only to improve the accuracy of numerical ocean wave prediction, but also to combine the wave model with a coupled ocean-atmosphere model. Since the ocean wave hindcast by the model will reduce the systematic errors of visually-observed data, ocean wave statistics by means of wave hindcasts will be useful in many branches of shipbuilding or marine transport.

## Acknowledgments

I wish to express my special thanks to Dr. I. Isozaki of Japan Weather Association for his advice and encouragement throughout the present study. I also wish to express my thanks to Professor H. Mitsuyasu of Hiroshima Institute of Technology, Professor Y. Toba of Tohoku University, Professor R. Hosoda of University of Osaka Prefecture, Professor R. Kimura of University of Tokyo and Professor A. Masuda of Kyushu University for their discussions and valuable comments on this study. I gratefully acknowledge Professor Y. Tsuji of University of Tokyo for reading the manuscript and giving valuable comments. Thanks are also extended to my colleagues of Japan Weather Association for their advice and suggestions.

# Contents

## 1. Introduction

The prediction of ocean waves is essential for human activities in the ocean, because of ocean waves are a major cause of maritime disasters. It is generally recognized today that ocean wave prediction is second most accurate among natural phenomena, next to tidal prediction. However, studies of ocean wave prediction were developed only during the last five decades.

Routine work of numerical ocean wave prediction by the Japan Meteorological Agency (JMA) was started in March 1977, by introducing the MRI model proposed by Isozaki and Uji (1973). MRI was replaced by MRI-II (Uji, 1984) in September 1986 and is still being used by JMA. Although the accuracy of these wave models is practical enough, more accurate ocean wave predictions over long periods are needed for the purposes of prevention of maritime disasters, the safety of large marine structures, economical ship routing, etc. In addition to the traditional wave parameters, a directional ocean wave spectrum is needed so as to predict the response of maritime structures and ships to the wave fields.

Though there were many discussions about the role of ocean waves in air-sea interactions, a precise solution to this problem was not established yet. The problem of sea surface roughness is essential as a basic problem which is related to momentum transport, heat transport and mass exchange including carbon dioxide across the sea surface. But most empirical relations for sea surface roughness are functions of only wind speed at the sea surface, whereas it is possible to consider that the sea surface roughness may also be dependent on the wave parameters.

With respect to the relation between sea surface roughness and wave parameters, Kitaigorodskii and Volkov (1965) first proposed the concept of wave age as an effective parameter for the sea surface roughness. The wave age is expressed as $C/u_*$ in which $C$ is a phase speed of the wave and $u_*$ is a friction velocity of the wind.

Most of the parameterization schemes, such as Charnock's (1955) well known formula for the sea surface roughness, that were incorporated into the boundary schemes of atmospheric models, were independent of the wave age. However, if the dependence of sea surface roughness on the wave parameters becomes established, a more highly

accurate ocean wave model will be required so as to estimate the wave parameters. Weber (1994) discussed the effect of the wave parameters on the results of climate models by means of coupling an ocean wave model with a climate model.

Considerable progress was made in the field of remote sensing technology from satellites as a way to observe global environmental conditions. The radar altimeter can provide a measure of the significant wave height parameter through the distortion of the mean shape of the return pulse, though the other wave parameters can not be measured (Townsend *et al.*, 1981). After the successful results of measuring wave height by the SEASAT altimeter in 1978, further satellites named GEOSAT (1985), ERS-1 (1991) and Topex/Poseidon (1992) were launched. They provided many observed data of wave height. The accuracy of wave height measurement is evaluated as the greater value of either 0.5 m or 10 % of the significant wave height (Dobson *et al.*, 1987). We can improve the accuracy of ocean wave prediction by means of the assimilation of satellite data into an ocean wave model (*e.g.*, Janssen *et al.*, 1989; Lionello *et al.*, 1992). Since the results from the wave model must be used as the first estimated value, especially in areas without any wave measurements, the satellite data assimilation becomes more essential. We can suppose that the satellite data assimilation system will be adopted in future as part of the routine operation of numerical ocean wave prediction. The study of ocean wave modeling is the first step towards this goal of data assimilation.

In addition to the necessity of developing a highly accurate ocean wave model, which can be executed as a routine operation, a research study of global ocean wave characteristics with applying ocean wave models is required. In shipbuilding, marine transport and marine construction, not only information on tides and tidal currents, but also information on sea surface wind, wind waves and swell are the most essential information, in order to estimate the natural background conditions. The ocean wave statistics of the whole globe for as long a period as possible is needed for the purpose of the seaworthy design of ships and marine structures or for planning the schedules for marine constructions.

Ocean wave statistics based on visual observation were discussed by Hogben and Lumb (1967), Yamanouchi and Ogawa (1970), Takaishi *et al.* (1980) and Hogben *et al.* (1986). However, the visually-observed data contain systematic errors, because the

visual observation of ocean waves has the problems of lack of objectivity due to differences between individual observers; lack of observing points in areas away from the regular course of ships; and a decline in the frequency with which severe storms are encountered, due to keeping away from storms for the safety of ships. In order to overcome these difficulties, the method of the ocean wave hindcast applying an ocean wave model became of major interest lately (*e.g.*, Yamanouchi, 1989; Suzuki, 1994).

The method of hindcast had primarily been applied as a way of obtaining design conditions of ocean wave height for the purpose of constructing harbors. The ocean wave field in any given meteorological conditions can be reproduced by means of the wave model, in which analyzed sea surface wind data from weather charts are used as the wind force in the model. FNOC (Fleet Numerical Oceanography Center, USA) attempted to derive statistics of ocean waves applying the hindcast method in 1976. The object of this project was the improvement of the seaworthiness of warships. The first generation wave model SOWM (Lazanoff *et al.*, 1973) was applied. Part of the results of the project was quoted as a comparison data in Hogben *et al.* (1986). Tomita *et al.* (1992) also derived statistics of ocean waves in the north Pacific Ocean applying the hindcast method, using the second generation wave model MRI-II (Uji, 1984) combined with observed data from ships and buoys.

Naturally, the accuracy of the ocean wave hindcast depends on the completeness of the ocean wave model itself. In addition, it depends on the accuracy of the sea surface wind field which acts on the ocean wave field as an external force. Therefore, if accurately analyzed data of the global sea surface wind field are available, we can accurately reproduce the global ocean wave field.

In meteorological offices in some countries, as well as JMA, a global atmospheric analysis model is operated routinely so that analyzed global atmospheric data are accumulated day by day. Since the operation of a global atmospheric model in JMA was started in March 1988, the data stock is not large enough to study the statistics of global ocean wave characteristics. On the other hand, in NMC (National Meteorological Center, USA) or in ECMWF (European Centre for Medium-range Weather Forecasts), the global atmospheric models are operated routinely from the latter half of the 1970s, so that stock of analyzed global atmospheric data are available for a period of more than

ten years.

The motivation for studying global ocean wave characteristics applying ocean wave modeling becomes greater recently, for the following reasons: an increase of the social demand to develop a highly accurate wave model by which the global ocean wave characteristics are predictable; an increase in the amount of analyzed wind data that were stocked over a long period of time; and the appearance of a third generation wave model based on the latest research results on the physical processes of wave generation (*e.g.*, WAMDI Group, 1988). The objective of the present paper is to establish the method of prediction of global ocean wave field and to study global ocean wave characteristics based on hindcast results obtained by using the ocean wave model. In the first, we develop a new global ocean wave model including nonlinear interactions and dissipation. Next, the new ocean wave model is applied to hindcast the global ocean wave field over a long period of time, and finally we study the global ocean wave characteristics based on the hindcast results. The development of a newly proposed third generation wave model with a highly accurate scheme will be effective not only for increasing the accuracy of numerical ocean wave prediction, but also for improving the accuracy of a coupled ocean-atmosphere model with combining the wave model into that. Since the results of this study will help to overcome the problem of systematic errors in visually observed data, ocean wave statistics by means of the wave model will be useful in many branches of shipbuilding and marine transport.

In the present paper, a historical review of ocean wave modeling is given in Chapter 2. The development of a new third generation wave model JWA3G and its basic characteristics are described in Chapter 3. In Chapter 4, a global ocean wave hindcast over ten years is described and its verified results are discussed. The analysis of the global ocean wave characteristics is discussed in Chapter 5. The concluding discussion of the present paper is given in Chapter 6.

## 2. Historical review of ocean wave modeling

Ocean wave modeling has been progressing rapidly during the past 50 years, due to the development of the statistical description of ocean waves and to progress in basic research in the physical processes of wave generation, growth and dissipation. In this chapter, pioneer work in ocean wave modeling is described in section 2.1, and the classification of wave models is described in section 2.2.

### 2.1 Pioneer work on ocean wave modeling

Ocean wave prediction becomes of general interest as a problem related directly to human activity in the ocean. The study of scientific ocean wave prediction started with Sverdrup and Munk (1947). The study of ocean wave prediction made rapid progress for about 50 years (*e.g.*, Kinsman, 1965; Nagata, 1971; Taira, 1975; Isozaki, 1990; Mitsuyasu, 1995). The history of the study of ocean wave prediction is summarized in Figure 2.1.

The theory of Sverdrup and Munk (1947) was epoch-making for the following reasons:

a) They introduced the concept of the "significant wave", which was defined as a statistical mean value, in order to describe the random ocean wave field quantitatively.

b) They proposed a theoretical framework of the process of wave generation, growth, propagation and dissipation.

c) They proposed a practical method of ocean wave prediction, resulting from a systematic study of fragmentary observed data.

This imaginary "significant wave" behaves as a kind of surface wave as well as a deep water wave with infinitesimal amplitude; however, its wave height and period are treated as dependent variables of time and space. We can regard that significant wave height is approximately equal to the visually observed wave height.

Sverdrup and Munk (1947) considered whether the wave slope $\delta = H/L$ ($H$ is wave height, $L$ is wave length) changed according to the wave age $\beta = c/U$ ($c$ is phase speed of the wind wave, $U$ is wind speed). They obtained the results shown in Figure 2.2 after arrangement of the visually observed ocean wave data. Their ocean wave

prediction method was called a parameter method, because the method was described using a few parameters such as wave height, wind speed, fetch and duration. This empirical formula for wave prediction was reformulated completely by Bretschneider (1952,1958) and Wilson (1961,1965) by means of highly accurate wave observational data which were available by then, so that the method was called the SMB method (taking the initial letters of Sverdrup, Munk and Bretschneider). Figure 2.3 shows the relation between non-dimensional fetch and non-dimensional wave height of wind waves based on the observational results (Wilson, 1965). Wilson (1965) derived the following relations for wind-wave prediction, and the relations are called the Wilson Ⅳ formula:

$$\frac{gH_{1/3}}{U_{10}^2} = 0.30\left\{1-\left[1+0.004\left(\frac{gF}{U_{10}^2}\right)^{1/2}\right]^{-2}\right\}, \tag{2.1}$$

$$\frac{gT_{1/3}}{2\pi U_{10}} = \frac{C_{1/3}}{U_{10}} = 1.37\left\{1-\left[1+0.008\left(\frac{gF}{U_{10}^2}\right)^{1/3}\right]^{-5}\right\}, \tag{2.2}$$

where $H_{1/3}, T_{1/3}$ and $C_{1/3}$ are the significant wave height (m), wave period (sec) and phase speed (m/s), respectively. $F$, $g$ and $U_{10}$ are the fetch (m), the gravitational acceleration (m/s$^2$) and wind speed (m/s) at 10 m height. The equations (2.1)-(2.2) reflect the fact that the non-dimensional wave height and wave period gradually approach limiting values and become saturated when the non-dimensional fetch is large enough. The physical meaning is explained as follows: As the wind wave grows, the wave period becomes longer, so that the phase speed increases. The approach of the phase speed to the wind speed results in the decrease of momentum transport from wind to wave, because the wind speed relative to the phase speed becomes smaller. Thus wind waves do not grow any more in the saturated stage in which the energy from wind and dissipation by wave breaking are balanced. Present ocean wave prediction models follow the above framework based on the energy balance in ocean waves.

Since this simple Wilson Ⅳ formula is available for ocean wave prediction under the simple conditions of a uniform wind field and limited fetch, with sufficient accuracy,

it is still applied widely in the field of coastal engineering. Its application to numerical prediction method on a grid system was reported by Ijima *et al.* (1967).

While the ocean wave prediction method based on the parameters of ocean waves was improved, the statistical theory to describe the random wave field was developed rapidly on the other (*e.g.*, Longuet-Higgins, 1952; Cartwright and Longuet-Higgins, 1956), owing to the influence of the development of the mathematical analysis of random noise in electrical engineering (*e.g.*, Rice, 1944). Cartwright and Longuet-Higgins (1956) derived theoretically the statistical distribution of the maximum surface elevation $\eta(t)$, based on the assumption that in addition to the distribution of $\eta(t)$ and its derivatives $\dot{\eta}(t)$ and $\ddot{\eta}(t)$, its joint distribution are normal Gaussian processes. The distribution of maximum surface elevation approached the Rayleigh distribution $P(\varsigma) = \varsigma \exp\left(-\varsigma^2/2\right)$ ($\varsigma$ is a normalized value of $\eta(t)$ using the 0th moment $m_0$ of the wave spectrum) in the limit of an infinitely narrow spectrum. On the basis of the assumption that the wave height obeyed a Rayleigh distribution, the representative relations between mean wave height $\overline{H}$, significant wave height $H_{1/3}$ and 0th moment $m_0$ were derived (Cartwright and Longuet-Higgins, 1956):

$$\overline{H} = \sqrt{2\pi m_0}\ , \tag{2.3}$$

$$H_{1/3} = 1.597\sqrt{2\pi m_0} = 4\sqrt{m_0}\ . \tag{2.4}$$

This statistical theory led to the development of ocean wave prediction based on the wave spectrum, because the significant wave height was connected with the wave spectrum based on the theory.

In addition, the study of ocean wave prediction based on the ocean wave spectrum was developed through the improvement of the method of observing the wave spectrum. Barber and Ursell (1948) studied the relation between storms in the Atlantic Ocean and the wave spectrum observed at the west coast of England. They suggested the possibility of ocean wave prediction based on the assumption that each spectral wave component propagates independently according to its group velocity. Their study was succeeded by Darbyshire (1955) and it became the basis for the ocean wave prediction method in

England.

Neumann (1953) obtained an empirical formula which gave an upper limiting value of wave slope, by means of a systematic analysis of some observed ocean wave data. The wave spectrum (Neumann spectrum) was derived from the empirical formula for wave slope according to physical considerations of the translations of the wave slope into the spectrum. The ocean wave prediction method based on the Neumann spectrum was named the PNJ (Pierson, Neumann and James, 1955) method. Since the PNJ method was superior to other methods as a concept of ocean wave prediction based on the wave spectrum, it was a good chance for many scientists to do theoretical and experimental research on wave generation and growth more actively. The concept of the PNJ method is as follows.

In the PNJ method, we assume that a fully developed ocean wave spectrum is given in the form of the Neumann spectrum. This spectrum increases from high frequency to low frequency depending on the wind, as shown in Figure 2.4. If the wave growth is restricted by the fetch and duration, the low-frequency part of the spectrum except the shaded area in Figure 2.4 (upper) is excluded, depending on the amount of wave growth. We also assume that the directional distribution of the ocean wave spectrum is proportional to $\cos^2\theta$. If the directional ocean wave spectrum is determined as mentioned above, we can express the propagation of ocean waves, assuming that each wave component propagates independently at its corresponding group velocity.

The problem that the SMB method found it difficult to express the swell propagation was solved with the PNJ method. But there was not enough computing power to process the calculations of the PNJ method at that time, so that a simple chart for the prediction of ocean waves such as Figure 2.5 was made for convenience. The chart shows cumulative ocean wave spectra, which are integrated from high frequency to low frequency of the Neumann spectrum according to the wind speed, and the curves describe the limits of fetch and duration. If the wave energy $E$ is read off the figure, we can estimate the significant wave height by using the relations of Cartwright and Longuet-Higgins (1956). Baer (1962) developed a computer code to process ocean wave calculations applying the PNJ method.

There is a difference between the SMB and PNJ methods in the way of expressing the ocean wave fields either by significant wave height or by the wave spectrum. Both of them are based on the relations between ocean waves and wind when the wave field reaches a saturated state under the condition of a uniform wind field. From the point of view of the energy transport equation, which dominates the ocean wave growth, this way of thinking is based on the integrated results of the energy transport equation under the condition of a uniform wind field. Therefore it is very difficult to apply both the SMB and PNJ methods to wind fields which vary in time and space. For this reason, the ocean wave prediction methods based on the energy transport equation were developed in the beginning of the 1960s.

Since the pioneer work by Gelci *et al.* (1956), numerical ocean wave prediction models have been formulated in terms of the energy transport equation for the two-dimensional ocean wave spectrum. Gelci *et al.* (1956) considered the idea of the energy spectral density (DSA: Densité Spectrale Angulaire) of ocean waves and proposed a numerical ocean wave prediction method applying a simplified energy transport equation. But the spectral density was defined as a function of wave period and direction, and there was not enough physical understanding of the process of ocean wave growth and decay.

Hasselmann (1960) proposed an energy transport equation for the ocean wave spectrum, in which the physical processes of wave growth and decay were considered separately. The equation became a prototype of many of the currently-used ocean wave models. The evolution of the two-dimensional ocean wave spectrum $F(\omega,\theta)$ with respect to angular frequency $\omega$ and direction $\theta$ is governed by the energy transport equation

$$\frac{\partial F(\omega,\theta)}{\partial t} + \nabla \cdot \boldsymbol{C}_g F(\omega,\theta) = S_{net}(\omega,\theta) , \qquad (2.5)$$

where $\boldsymbol{C}_g$ is the group velocity. The first and second terms on the left-hand side of (2.5) describe the local change of the two-dimensional ocean wave spectrum and the divergence of the wave energy flux, respectively. $S_{net}(\omega,\theta)$ on the right-hand side is a general description of energy input and output source functions corresponding the wave

energy changes, and is called the energy source function. Hasselmann (1968) showed that the energy transport equation should be subject to slowly-varying conditions in time and space. The conditions are expressed as

$$\frac{1}{\omega}\frac{\partial F}{\partial t} \ll 1\,, \quad \frac{1}{k}\frac{\partial F}{\partial x} \ll 1\,, \tag{2.6}$$

where $t$ ,$x$ and $k$ are time, space and wave number, respectively.

The net energy source function $S_{net}$ is related to the basic physical processes of ocean wave generation and dissipation, and is generally represented as the sum of three physical processes:

$$S_{net} = S_{in} + S_{nl} + S_{ds}\,. \tag{2.7}$$

$S_{in}$ is the energy input by the wind, $S_{nl}$ the nonlinear energy transfer due to resonant wave-wave interactions, and $S_{ds}$ is the energy dissipation due to wave breaking, bottom friction, etc. If each spectral component of the source functions $S_{in}$, $S_{nl}$ and $S_{ds}$ are given as functions of time and space, we can estimate the evolution of ocean wave fields by means of integrating equation (2.5) under the proper initial and boundary conditions. Since each source function is generally defined as a nonlinear function of the wave spectrum $F(\omega,\theta)$, it is necessary to use a numerical simulation method instead of integrating equation (2.5) analytically.

There are many types of wave models which differ according to the treatment of the energy source functions, whether shallow or deep water, and the numerical procedures adopted to solve the energy transport equation. SWAMP Group (1985) classified various ocean wave models systematically and put together the intercomparison studies. The results are described in section 2.2. In other words, the main developments in ocean wave modeling since the 1960s was the history to clarify the physical processes of each energy source function.

With respect to the energy input by the wind, Ursell (1956) attracted the interest of many researchers to study the processes of wind-wave generation. Phillips (1957) proposed a theory of wind-wave generation by a resonance mechanism between a random distribution of normal pressure, and wind waves. In the same year, Miles (1957)

proposed a theory in which the momentum of a parallel shear flow was transported downward due to the instability which occurred in the critical layer where the wind speed was equal to the phase speed of the ocean wave. But it was found that the observed growth rates of actual ocean wind waves were one order of magnitude larger than those predicted by Miles' theory (*e.g.*, Snyder and Cox, 1966; Barnett and Wilkerson, 1967). Therefore, the empirical relations based on the observed results from a wind-wave tunnel (*e.g.*, Mitsuyasu and Honda, 1982) or ocean wave observations (*e.g.*, Snyder *et al.*, 1981) were adopted. Inoue (1967) obtained relations for the energy transport from wind to waves after arrangement of observed wave spectra. However, the results were equivalent to the sum of both $S_{in}$ and $S_{nl}$. With respect to theoretical work on the generation of wind waves after Phillips (1957) and Miles (1957), Kawai (1979) proposed a theory of the generation of initial waves by the instability of a coupled shear flow, and Miles (1993) modified his own previous theory (1957) to incorporate the wave-induced perturbations of the Reynolds stresses. Miles (1993) showed agreement with the observational data compiled by Plant (1982). After the latter half of the 1980s, attempts to obtain the energy transport from the wind to waves by means of numerical simulation of the turbulent closure models were carried out (*e.g.*, Al-Zanaidi and Hui, 1984; Duin and Janssen, 1992).

After Phillips (1960) first studied the nonlinear energy transfer $S_{nl}$, Hasselmann (1962) studied analytically the rate of nonlinear energy transfer due to resonant wave-wave interactions at the fourth order of the wave slope. But it is quite impossible to incorporate an explicit calculation scheme for the nonlinear energy transfer into a practical ocean wave model, because the explicit calculation of $S_{nl}$ which is represented by a cubic integral in wave number space requires an enormous amount of computational calculation, even using a supercomputer. For this reason, coupled hybrid wave models were developed. The nonlinear energy transfer mechanism in the coupled hybrid models are represented by a simple parameterization of $S_{nl}$ such as Barnett (1968) or by using an implicit expression for $S_{nl}$ making use of the self-similarity structure of the wind-wave spectrum. Since the coupled hybrid models had difficulty in separating wind-wave energy from swell energy, a wave model with an explicit

calculation scheme for $S_{nl}$ was required (SWAMP Group,1985). To meet this requirement, Hasselmann *et al.* (1985) developed an approximate calculation scheme for the nonlinear energy transfer. The WAM model (WAMDI Group, 1988) was developed based on the results of Hasselmann *et al.* (1985).

In the process of energy dissipation, it is assumed that wave breaking plays the most principal role, but its analytical and experimental studies are not sufficiently made. Therefore the energy dissipation of many wave models is expressed by a simple and artificial scheme, by means of restricting the growth of the wave spectrum by applying a standard saturated spectrum: the PM spectrum (Pierson and Moskowitz, 1964) or the JONSWAP spectrum (Hasselmann *et al.*, 1973).

The PM spectrum was formulated by constructing an empirical ocean wave spectrum on the assumption that the equilibrium range of the wind wave spectrum is expressed as the $f^{-5}$ law by Phillips (1958). He assumed that the physical processes in the equilibrium range of the wind-wave spectrum are dominated by wave breaking only, so that the energy input by the wind is not essential, and the gravitational acceleration is the only forcing term. By means of a dimensional analysis, the dimensions of the ocean wave spectrum $F$, the gravitational acceleration $g$ and the frequency $f$ are expressed by $[F] = L^2T$, $[g] = LT^{-2}$ and $[f] = T^{-1}$, respectively, where $L$ and $T$ denote length and time. By substituting these equations into the relation $[F] = [g]^n[f]^m$, a formula for the equilibrium range of the wind-wave spectrum is easily derived as $F(f) \propto g^2 f^{-5}$. The JONSWAP spectrum was obtained by Hasselmann *et al.* (1973) by means of analyzing the ocean wave spectra observed by the Joint North Sea Wave Project in the North Sea. The basic form of the JONSWAP spectrum was the same as the PM spectrum, but it was modified so as to express the energy concentration around the peak of the spectrum.

Hasselmann (1974) first proposed a formula for the energy dissipation by analyzing the results of the observed random pressure distribution working at the ocean wave surface. Komen *et al.* (1984) derived an expression for the energy dissipation by means of a numerical simulation of the energy transport equation, in which only the energy dissipation was treated as an unknown term, while the energy input by the wind was as represented by Snyder *et al.* (1981), and an exact calculation of the nonlinear energy

transfer was made. The energy dissipation term which gave the best agreement with the observed PM spectrum was adopted. The energy dissipation by Komen *et al.* (1984) was incorporated into the WAM model. This way of thinking based on the energy balance between the energy source functions was systematically studied by Phillips (1985), and some studies to formulate the energy dissipation based on this theory have been attempted (*e.g.*, Banner and Young, 1994; Melville, 1994).

As mentioned above, theoretical and experimental studies on the basic physical processes governing the evolution and dissipation of ocean waves are insufficient. Nevertheless, it is satisfying to consider that the accuracy of ocean wave prediction by wave models is good enough to be of practical application, because some empirical relations of the ocean waves are skillfully incorporated into the wave models.

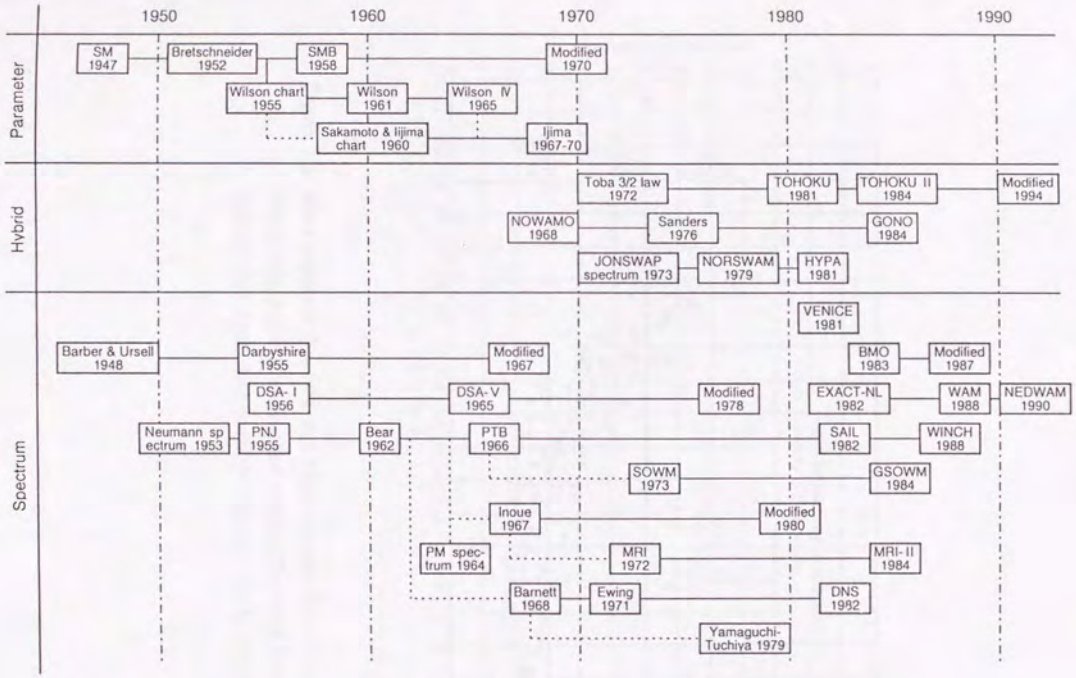


**Figure 2.1** Historical development of ocean wave modeling.
The latest studies are added to the figure of Isozaki (1974).

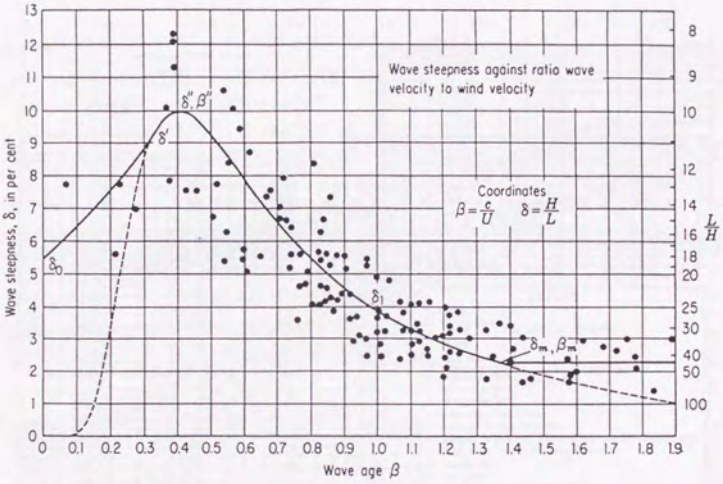


**Figure 2.2** Wave steepness $\delta = H/L$ as a function of wave age $\beta = c/U$. The plotted points are observed results. The solid line is the assumed functional relation (from Sverdrup and Munk, 1947).

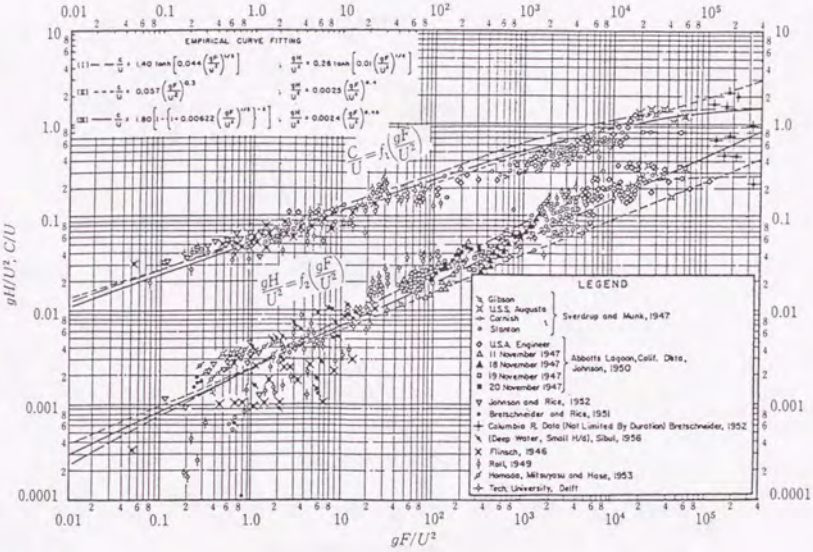


**Figure 2.3** Nondimensional relations governing wind wave growth. Nondimensional wave height $gH/U^2$ and wave period $C/U = gT/2\pi U$ are plotted against nondimensional fetch $gF/U^2$ (from Wilson, 1965).

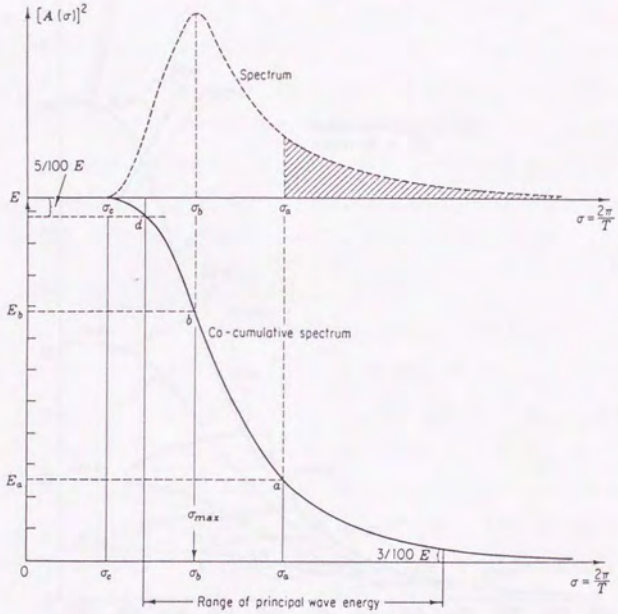


**Figure 2.4** Relations between ocean wave spectrum (upper) and co-cumulative spectrum (below) (from Pierson *et al.*, 1955).

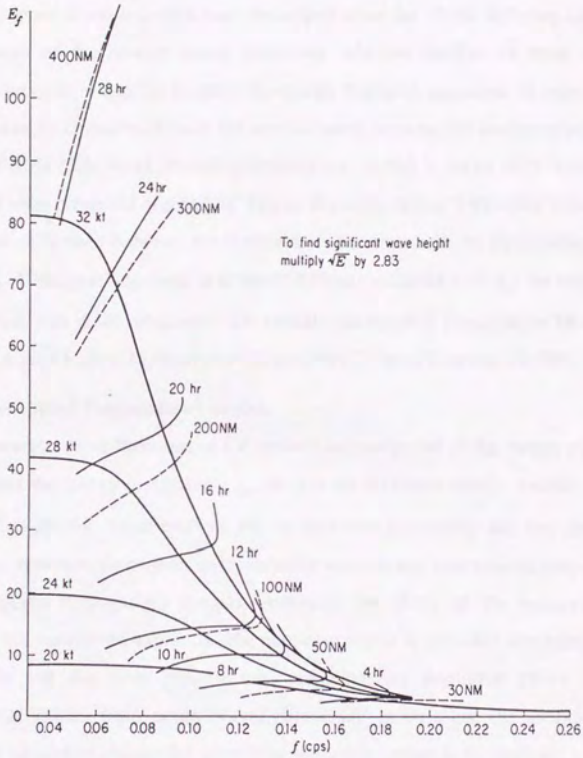


**Figure 2.5** Example of co-cumulative spectrum with combined graph of fetch and duration (from Pierson *et al.*, 1955).

## 2.2 Classification of ocean wave models

Many types of wave models were developed since the 1960s, differing according to the treatment of the energy source functions, whether shallow or deep water and numerical procedures applied to solve the energy transport equations. In order to clarify the difference of characteristics of the several wave models, the intercomparison study named SWAMP (Sea Wave Modeling Project) was started in about 1979. The results of the project were presented in detail in "Ocean Wave Modeling" (SWAMP Group, 1985). The largest difference between wave models is the treatment of the nonlinear energy transfer $S_{nl}$. Distinguishing them in terms of different treatments of $S_{nl}$, the wave models are classified into three categories: DP models (Decoupled Propagation Models), CH models (Coupled Hybrid Models) and CD models (Coupled Discrete Models).

**(1) DP (Decoupled Propagation) models**

The energy source functions of DP models are composed of the energy input by the wind $S_{in}$ and the energy dissipation $S_{ds}$, so that the nonlinear energy transfer $S_{nl}$ is not considered explicitly. Since each of the components composing the two-dimensional ocean wave spectrum propagates independently without any interactions, they are called DP (Decoupled Propagation) models. Although the effect of the nonlinear energy transfer is not considered explicitly, the nonlinear effect is included implicitly, because DP models use the total growth rate including the nonlinear effect based on observational results from ocean waves. Since DP models use the artificial energy dissipation scheme to restrict the growth of the wave spectrum by applying a saturated spectrum (*e.g.*, PM spectrum) as a limiting value, the models have enough accuracy for practical use. Even though DP models have two weak points. One is the difference of an order of magnitude between the energy input of the model and that obtained by ocean wave observations and wind-wave tunnel experiments, because the energy input of DP models includes the effect of the nonlinear energy transfer implicitly. The other is the fact that the model is not able to reproduce the overshoot and undershoot phenomena which can be observed in the actual ocean wave spectrum (*e.g.*, Barnett and Sutherland, 1968). This refers to the observation that the spectral component of wave energy around the peak fluctuates in time and space as it gradually approaches the saturated value.

Typical DP models were DSA (Gelci *et al.*, 1956), PTB (Pierson *et al.*, 1966), SOWM (Lazanoff *et al.*, 1973) of the US Navy which was an improved version of PTB, GSOWM (Clancy *et al.*, 1986) a global version of SOWM, Inoue (1967) which was developed at New York University and MRI (Isozaki and Uji, 1973) which was used for a long time as an operational ocean wave prediction model by JMA (Japan Meteorological Agency). The wave models of Barnett (1968) and Ewing (1971) introduced an explicit representation of $S_{nl}$ by means of a simple parameterization of the nonlinear effect for the Neumann spectrum. However, they were classified as DP models, because the nonlinear effects were one order of magnitude smaller than other source terms and the models were governed mainly by the energy input by the wind. Let us take the MRI model (Isozaki and Uji, 1973) as an example to show the details of a DP model.

The MRI model which was developed by Isozaki and Uji (1973) started to be used as an operational numerical ocean wave prediction model by JMA from March 1977, after many examinations for practical application of the model together with the development of a numerical model of sea surface winds (Isozaki and Uji, 1974). The model was used for about ten years until it was replaced by MRI-II (Uji, 1984) in September 1986. The accuracy of the model was highly rated.

In the MRI model, the energy source functions of the linear growth by the wind (Phillips' mechanism), exponential growth by the wind (Miles' mechanism), and energy dissipation due to wave breaking, internal friction (eddy viscosity) and adverse wind, are considered. Though the effect of nonlinear energy transfer $S_{nl}$ is not considered explicitly, it can be considered that the nonlinear effect is included implicitly by applying the growth relation of Inoue (1967), in which the nonlinear effect $S_{nl}$ is not separated from the wind input $S_{in}$. The model is based on the assumption of the existence of a fully-developed ocean wave spectrum, which is expressed by the PM spectrum (Pierson and Moskowitz, 1964):

$$F_{PM}(f) = \alpha g^2 (2\pi)^{-4} f^{-5} \exp\left[-\beta\left(\frac{g}{2\pi u_{19.5}}\right)^4 f^{-4}\right], \tag{2.8}$$

where $g$ is the gravitational acceleration, $f$ the frequency and $u_{19.5}$ is the wind speed at 19.5 m height. $\alpha$ and $\beta$ are constants with $\alpha = 8.1 \times 10^{-3}$ and $\beta = 0.74$, respectively. The constant $\alpha$ is called Phillips' constant.

The energy source function $S_{net}$ takes different forms according to wind conditions of favorable and adverse wind. It is represented as follows.

Favorable wind case: $|\theta - \theta_w| \le 90^\circ$

$$S_{net} = \left[A + B \cdot F(f,\theta)\right] \cdot \left[1 - \left(\frac{F(f,\theta)}{F_{PM}(f,\theta)}\right)^2\right] G(\theta - \theta_w) \ , \qquad (2.9)$$

$$S_{net} = -D f^4 F(f,\theta) \ . \qquad \begin{matrix} F(f,\theta) \le \sqrt{2} F_{PM}(f,\theta) \\ F(f,\theta) > \sqrt{2} F_{PM}(f,\theta) \end{matrix} \qquad (2.10)$$

Adverse wind case: $|\theta - \theta_w| > 90^\circ$

$$S_{net} = -\left[B \cdot G(\theta - \theta_w) + D f^4\right] F(f,\theta) \ . \qquad (2.11)$$

Here $\theta$ is the wave direction, $\theta_w$ the wind direction, $F(f,\theta)$ the two-dimensional ocean wave spectrum and $G(\theta - \theta_w)$ is the directional distribution function proportional to $\cos^2(\theta - \theta_w)$. The terms $A$ and $B$ are the linear and exponential growth of wind waves derived by Inoue (1967):

$$A(f,u) = \int_{-\pi/2}^{\pi/2} \frac{3.54 \times 10^{-11} \omega^{5.25} u^{2.25}}{\left[\frac{1}{4}\left(\frac{\omega}{u}\right)^2 + (k \sin\theta)^2\right]\left[\frac{1}{9}\left(\frac{\omega}{u}\right)^{2.5} + \left(k\cos\theta - \frac{\omega}{u}\right)^2\right]} d\theta \ , \qquad (2.12)$$

$$B(f,u_*)/f = 5e^{-7000\left(\frac{u_*}{c} - 0.031\right)^2} + 2612\left(\frac{u_*}{c}\right)^2 e^{-0.0004\left(\frac{u_*}{c}\right)^{-2}} \ , \qquad (2.13)$$

where $u$ is the wind speed at 19.5 m height, $u_*$ the friction velocity, $c$ the phase speed of each spectral component and $k$ is the wave number. The term $D$ in equations (2.10) and (2.11) is the coefficient of internal friction (eddy viscosity), which is selected to be $D = 1 / 3600 \ \mathrm{sec}^3$ so that the wave components shorter than three seconds will disappear within one hour if there is no energy input by the wind.

The energy transport equation (2.5) is transformed into a difference equation and integrated numerically. In the calculation of the energy propagation term of the MRI

model, a coupled numerical scheme of the finite difference method and jumped method is applied. The jumped method was adopted in the PTB model (Pierson *et al.*, 1966) in which the wave energy remains at a particular grid point until enough time has elapsed so that the energy can reach the vicinity of the neighboring grid point. The resolution of direction in MRI is a coarse 16 directions, so that the energy propagation tends to have an anisotropy because of only using a finite difference method. Therefore the jumped method is applied in combination with the energy propagation scheme so as to realize isotropic propagation. However, the jumped method has a weak point in that the propagated energy distribution becomes too broad. Also, its application to different coordinate systems such as spherical coordinates is difficult, because the jumped method distributes the wave energy by multiplying a neighboring wave energy by defined coefficients.

In DP models similar to MRI, the form of the wave spectrum is made to gradually approach a fully-developed spectrum (*e.g.*, PM spectrum) by multiplying the source function by the factor $\left[1-\left(F/F_{PM}\right)^2\right]$ in equation (2.9). This $-\left(F/F_{PM}\right)^2$ factor can be understood as an implicit expression for the energy dissipation.

**(2) CH (Coupled Hybrid) models**

In CH models, the wind wave component is expressed in terms of a few parameters based on the observed results, that the spectra of growing wind waves appear to have an approximately self-similar shape for a wide variety of generation conditions, while the models treat the swell components in the same way as DP models, in which different wave components propagate independently. Since the models use a combined expression of the parameterized wind wave and independent swell components, they are called CH (Coupled Hybrid) models.

The self-similar shape of growing wind wave spectra had been considered as proportional to $f^{-5}$ (Phillips, 1958). However, many subsequent observations of ocean wave spectra showed that the shape was proportional to $f^{-4}$ (*e.g.*, Kawai *et al.*, 1977; Mitsuyasu *et al.*, 1980). The result that the shape of growing wind-wave spectra is proportional to $f^{-4}$ was first introduced by Kitaigorodskii (1962), based on dimensional analysis. Toba (1973) introduced that the shape of the wind-wave spectra which was

equivalent to the 3/2 power law (Toba, 1972) was proportional to $f^{-4}$. Phillips (1985) presented a new concept instead of his 1958 theory, in which the same $f^{-4}$ spectra as Kitaigorodskii (1962) and Toba (1973) was derived. The concept was based on the assumption that, in the equilibrium range, sum of three processes of energy input by the wind $S_{in}$, nonlinear energy transfer $S_{nl}$ and energy dissipation by wave breaking $S_{ds}$, was equal to zero: $S_{in} + S_{nl} + S_{ds} = 0$.

Since the evolution of wind-wave spectra occurs as a result of the total action of all the physical processes of $S_{in}$, $S_{nl}$ and $S_{ds}$, then if we can describe the evolution of wind-wave spectra in terms of several parameters on the basis of the self-similarity structure of the spectra, we can incorporate the processes of nonlinear energy transfer and energy dissipation, which are difficult to calculate individually, into the ocean wave models. CH models can be considered as more improved models than DP models, since CH models are based on the knowledge that the process of nonlinear energy transfer is essential.

CH models incorporate knowledge gained from experimental results on ocean waves into wave modeling; however, the application of experimental results is only restricted to the growth stage of wind waves. Therefore, the same treatments of energy dissipation and swell propagation as in DP models are needed. A significant disadvantage of CH models is the problem that there remains an arbitrariness in the separation of wind wave and swell, and the swell separation is sometimes difficult.

Typical CH models were GONO (Sanders, 1976; Janssen *et al.*, 1984) in The Netherlands, HYPA (Günther *et al.*, 1979) in Germany and TOHOKU (Kawai *et al.*, 1979; Joseph *et al.*, 1981a, 1981b; Toba *et al.*, 1985; Okada, 1994) developed in Tohoku University. Let us take the TOHOKU model as an example to show the details of a CH model.

The TOHOKU model is based on the single-parameter growth equation for wind waves proposed by Toba (1978). The concept of Toba (1978) is based on the hypothesis that the self-similarity structure of growing wind waves can be described using only one parameter $E^* \equiv g^2 u_*^{-4} E$, where $E$ is a wind-wave energy and $E^*$ is a value normalized by means of the friction velocity of the air $u_*$ and the gravitational acceleration $g$. The

single-parameter growth equation by Toba (1978) is expressed as

$$\frac{d\left(E^{*2/3}\right)}{dt^{*}} = G_0 R\left[1 - \mathrm{erf}\left(bE^{*1/3}\right)\right], \tag{2.14}$$

where $t^{*} \equiv g u_{*}^{-1} t$ is the non-dimensional time. $G_0 R = 2.4 \times 10^{-4}$ and $b = 0.12$ are the experimental constants. Here,

$$\mathrm{erf}(z) = \frac{2}{\sqrt{\pi}} \int_0^z \exp\left(-t^2\right) dt, \tag{2.15}$$

is the error function. Equation (2.14) shows that the wind wave energy is gradually approaching a limiting value obeying a probability process. Once the wind-wave energy is calculated by (2.14), we can estimate the corresponding wave height $H$ by the relation of Longuet-Higgins (1952),

$$E = H^2/16. \tag{2.16}$$

Wave period $T$ is obtained using the relation of the 3/2 power law (Figure 2.6) of Toba (1972),

$$H^{*} = B T^{*3/2}, \tag{2.17}$$

where $B = 0.062$ is an empirical constant, and $H^{*} \equiv g u_{*}^{-2} H$ and $T^{*} \equiv g u_{*}^{-1} T$ are the non-dimensional wave height and period, respectively. The wind waves can be considered as monotonic waves with period $T$, propagating with a group velocity $C_g = gT/4\pi$. The propagated wind-wave energy is interpolated to the neighboring grid points. If the wind is varying, an adjustment of wave energy is performed for the difference between wind direction and wave direction $\Delta\theta$.

$|\Delta\theta| \le 30^{\circ}$: All the wave energy $E$ propagates along the wind direction.

$30^{\circ} < |\Delta\theta| \le 60^{\circ}$: $E\cos^2\Delta\theta$ becomes the wind-wave energy and it propagates along the wind direction. The remaining energy $E\left(1 - \cos^2\Delta\theta\right)$ becomes swell propagating along the wave direction (Figure 2.7, swell partition 2).

$|\Delta\theta| > 60^{\circ}$: All the wave energy $E$ becomes swell and propagates along

the wave direction (Figure 2.7, swell partition 1).

The wind-wave component is then tested against the criterion $E > E_m$, where $E_m$ corresponds to $c/u_{10} = 1.37$ on the basis of the Wilson (1965) relation. The excess energy $E - E_m$ is transformed into the swell component. The swell component is divided into spectral components using Toba's spectrum (Joseph *et al.*, 1981a)

$$F(f) = \begin{cases} agu_* f^{-4}, & f > f_p \\ agu_* f_p^{-8} f^4, & f \le f_p \end{cases} \tag{2.18}$$

where $a = 9.6 \times 10^{-2}/(2\pi)^3$ is an empirical constant and $f_p$ is the peak frequency of the wave spectrum. Each swell component propagates independently with the energy dissipation due to internal friction (eddy viscosity) and adverse wind. The swell energy is transformed again into wind wave energy, if $\Delta\theta \le 60^\circ$ and $c/u_{10} \le 1.37$.

As mentioned above, by means of expressing the self-similarity structure as a single parameter, the TOHOKU model can incorporate the processes of nonlinear energy transfer and energy dissipation which are difficult to calculate individually into the ocean wave model. However, since the model adopts a somewhat artificial method with respect to the separation of wind waves and swell, it is a significant weak point of CH models that the distribution of wind-wave and swell components in time and space occasionally becomes discontinuous.

**(3) CD (Coupled Discrete) models**

There is a difference between CD models, and DP or CH models in that the nonlinear energy transfer $S_{nl}$ is expressed explicitly in some way. As previously stated, it is quite impossible to incorporate an explicit calculation scheme of the nonlinear energy transfer into a practical ocean wave model, because the explicit calculation of the nonlinear energy transfer, which is expressed by a cubic integral in wave number space, requires an enormous amount of computational calculation even though using a supercomputer. Therefore the numerical expression of the nonlinear effect in CD models is parameterized by the following methods, which are classified mainly into two categories.

a) The parameterized method in which the exact calculation results of $S_{nl}$ for a standard

wave spectrum (*e.g.*, JONSWAP spectrum) are expressed by a few parameters and the $S_{nl}$ term is estimated by finding the parameters which best fit the standard spectrum to the simulated spectrum (*e.g.*, Young, 1988).

b) The method in which the wave energy is redistributed so as to satisfy the self-similarity structure of growing wind waves, in the same way as in the CH model (*e.g.*, Golding, 1983; Uji, 1984).

Since both methods try to incorporate an explicit expression of the nonlinear effect into the ocean wave models, CD models can be considered as more improved models than CH models. However, the difference between CH and CD models is not always clear, since both models make use of the self-similarity structure of growing wind-wave spectra. In other words, the model which has more degrees of freedom for expressing the nonlinear effect is the CD model and the model with fewer degrees of freedom is the CH model.

An advantage of CD models is the parameterization of the nonlinear energy transport $S_{nl}$, but this advantage is possible to be a weak point itself. In ordinary circumstances, the spectral shape is rather complicated, such as when there is a double-peak spectrum with two wave components propagating in different directions, rather than the self-similar shape of growing wind waves. Since the nonlinear energy transfer for this complicated spectrum can not be fully represented by a simple parameterization based on the nonlinear effect for the standard spectrum, there is a weak point that an unreal and unstable spectrum can occasionally be calculated. If this unstable spectrum is stabilized by assuming the limit of a fully-developed wave spectrum, the advantage of CD models is reduced to the same order as that of CH models.

Typical CD models were MRI-II (Uji, 1984) which is used operationally in JMA, BMO (Golding, 1983) in the British Meteorological Office, SAIL (Greenwood *et al.*, 1985) and DNS (Allender *et al.*, 1985). Let us take MRI-II as an example to show the details of a CD model.

The MRI-II model developed by Uji (1984) is used operationally for numerical ocean wave prediction by JMA since September 1986. In the model, the same single-parameter growth equation by Toba (1978) as TOHOKU is incorporated. However, it is classified as a CD model, because the wind-wave energy is expressed by the individual

spectral components. The effect of the nonlinear energy transfer is expressed in terms of redistributing the wind-wave energy between the spectral components.

With respect to the wind-wave growth, Toba's (1978) growth equation applied to the PM spectrum is adopted:

$$\frac{d\sigma_p^{*-2}}{dt^*} = 1.783\times10^{-3}\left[1-\mathrm{erf}\left(4.59\times10^{-2}\sigma_p^{*-1}\right)\right]. \tag{2.19}$$

The non-dimensional angular peak frequency $\sigma_p^* = g^{-1}u_*\sigma_p$ obtained by equation (2.19) is substituted into the same relation as the PM spectrum

$$F^*\left(\sigma^*,\theta;\sigma_p^*\right) = \frac{\sigma_p^*}{\sigma_{PM}^*}\alpha\sigma^{*-5}\exp\left(-1.25\sigma_p^{*4}\sigma^{*-4}\right)\cos^2\theta\ , \tag{2.20}$$

which gives the non-dimensional wind-wave spectrum $F^*$. Here $\sigma_{PM}^* = (0.8\beta)^{1/4}g^{-1}u_*\sigma_0$ is the non-dimensional angular peak frequency of the PM spectrum, and $\sigma_0 = g/u_{19.5}$, $\alpha = 8.1\times10^{-3}$ and $\beta = 0.74$ are the constants. The directional distribution of the wind-wave spectrum is assumed to be proportional to a $\cos^2\theta$ distribution.

Energy dissipation by wave breaking, $S_{ds} = -Br\cdot F(\sigma,\theta)$ is expressed by using the probability $Pi$ derived from the observed proportion of whitecaps in the ocean (Toba and Chaen, 1973; Toba, 1979). The form of the breaking factor is expressed as

$$Br = C_b Pi\,\sigma_p E^2\left[1+\left(\sigma/2\sigma_p\right)^4\right]\Big/E_n\ . \tag{2.21}$$

Here, $E_n = \iint\left[1+\left(\sigma/2\sigma_p\right)^4\right]Fd\sigma d\theta$ is the normalization factor and $Pi$ is given as

$$Pi = 0.27\log\left(u_*^2/\sigma_p\nu\right)-0.78\ , \tag{2.22}$$

where $\nu$ is the kinematic viscosity of the air.

The energy source function $S_{net}$ is divided into two cases of favorable wind and adverse wind. They are expressed as follows.

Favorable wind case: $\left|\theta-\theta_w\right|\le 90^\circ$

$$S_{net} = \left[F^*\left(\sigma_p^*+\Delta\sigma_p^*,\theta\right)-F^*\left(\sigma_p^*,\theta\right)\right]\Big/\Delta t^*\ ,\ F(\sigma,\theta)\le F_{PM}(\sigma,\theta) \tag{2.23}$$

$$S_{net} = -\left[1 - \left(\frac{F(\sigma,\theta)}{F_{PM}(\sigma,\theta)}\right)^2\right] Br \cdot F(\sigma,\theta) \cdot$$

$$F_{PM}(\sigma,\theta) < F(\sigma,\theta) \le \sqrt{2}F_{PM}(\sigma,\theta) \qquad (2.24)$$

$$S_{net} = -Br \cdot F(\sigma,\theta) \qquad F(\sigma,\theta) > \sqrt{2}F_{PM}(\sigma,\theta) \qquad (2.25)$$

Adverse wind case: $|\theta - \theta_w| > 90^\circ$

$$S_{net} = -\left[B \cdot G(\theta - \theta_w) + D f^4 + Br\right] F(\sigma,\theta) \cdot \qquad (2.26)$$

Where $f$ is the frequency, $\sigma$ the angular frequency, $\theta$ the wave direction, $\theta_w$ the wind direction, $F(\sigma,\theta)$ the two-dimensional ocean wave spectrum and $G(\theta - \theta_w)$ is the directional distribution function proportional to $\cos^2(\theta - \theta_w)$. The term $B$ is the exponential growth rate of wind waves derived by Inoue (1967) as given by equation (2.13). In the calculation of energy propagation, the same coupled numerical scheme as in the MRI model is adopted.

The MRI-II model can express the growth of wind waves including implicitly the nonlinear effect in terms of the growth equation by Toba (1978), which is based on the assumption of the self-similarity structure of growing wind waves. But there remains the problem of the separation of swell energy from wind-wave energy and the problem of the expression of energy dissipation in which a limit of fully-developed wave spectrum is still applied.

The above three categories of DP, CH and CD models are the classification of ocean wave models by SWAMP Group (1985). The essential property of a CD model is defined as a model which expresses the nonlinear energy transfer explicitly, so that it is reasonable to call models which incorporate the nonlinear expression as precisely as possible proposed by Hasselmann (1962), CD models. Hasselmann *et al.* (1985) proposed an approximate and explicit calculation scheme for the nonlinear energy transfer (discrete interaction approximation) and the WAM model in which the approximate scheme was incorporated, was then developed (WAMDI Group, 1988). WAM is classified as a CD model according to the SWAMP Group (1985). The model is also called a third generation ocean wave model in the sense of being a new kind of model, because the number of degrees of freedom of the nonlinear scheme is significantly greater than that of the old CD models, and the growth limit of the wave

spectrum using a prescribed fully-developed spectrum is removed.

Corresponding to the third generation ocean wave models, there are also classifications of wave models called first and second generation wave models. In general, DP models which were developed from the 1960s to early 1970s are called first generation ocean wave models, and CD and CH models developed from the 1970s to 1980s are called second generation wave models. Although the definition of third generation wave models is ambiguous, it can be given as follows. A third generation wave model is a CD model, which employs discretized continuous operator parameterization of $S_{nl}$, containing the same number of degrees of freedom as used in the discrete representation of the spectrum. Typical third generation wave models are WAM (WAMDI Group, 1988), NEDWAM (Burgers, 1990) which is an application of WAM model to shallow water, and Boundary-WAM (Burgers and Makin, 1993), which is combined with the atmospheric boundary layer model. Both of the latter two models are recognized as modified version of WAM. The JWA3G model (Suzuki and Isozaki, 1994) which will be presented in this paper is also classified as a third generation ocean wave model. At present, WAM is the only third generation wave model except for JWA3G. The outline of WAM is as follows.

The WAM model is based on the energy transport equation in the spherical coordinate system for the purpose of calculating the global ocean wave field. The equation is expressed as

$$\frac{\partial F}{\partial t}+\frac{1}{\cos\phi}\frac{\partial}{\partial\phi}\left(\dot{\phi}\cos\phi F\right)+\frac{\partial}{\partial\lambda}\left(\dot{\lambda}F\right)+\frac{\partial}{\partial\theta}\left(\dot{\theta}F\right)=S_{nl}\,, \tag{2.27}$$

where $\phi$ is the latitude, $\lambda$ the longitude, $\theta$ the wave direction and $F(f,\theta,\phi,\lambda,t)$ is the two-dimensional ocean wave spectrum. $\dot{\phi}$ and $\dot{\lambda}$ are the group velocities in spherical coordinates for deep water :

$$\begin{cases}\dot{\phi}=\dfrac{C_g}{R}\cos\theta,\\ \dot{\lambda}=\dfrac{C_g}{R\cos\phi}\sin\theta.\end{cases} \tag{2.28}$$

$\dot{\theta}$ is the rate of change of the propagation-direction of a wave packet due to traveling along a great circle path:

$$\dot{\theta} = \frac{C_g}{R} \tan\phi \sin\theta \ . \tag{2.29}$$

The energy source function is represented as a superposition of the three physical processes: $S_{net} = S_{in} + S_{nl} + S_{ds}$. The energy input by the wind $S_{in}$ is adopted from Snyder *et al.* (1981) in the form

$$S_{in} = 0.25 \frac{\rho_a}{\rho_w} \left( 28 \frac{u_*}{c} \cos\theta - 1 \right) \omega F \ , \tag{2.30}$$

where $\omega$ is the angular frequency, $c$ the phase speed of the wave component, $\theta$ the difference between wave direction and wind direction, $\rho_a$ and $\rho_w$ are the densities of air and water, respectively.

The nonlinear energy transfer $S_{nl}$ is calculated explicitly by the discrete interaction approximation of Hasselmann *et al.* (1985). The discrete interaction approximation is expressed as

$$S_{nl}(\boldsymbol{k}_4) = \sum_{\gamma=1,2} A_\gamma \omega_4 \left[ n_1^\gamma n_2^\gamma \left( n_3^\gamma + n_4^\gamma \right) - n_3^\gamma n_4^\gamma \left( n_1^\gamma + n_2^\gamma \right) \right] , \tag{2.31}$$

where $A_\gamma$ are coupling coefficients and $n_i^\gamma \equiv F\left(\boldsymbol{k}_i^\gamma\right) / \omega_i^\gamma \ (i = 1,2,3 ; \gamma = 1,2)$ are the action densities. Equation (2.31) is an approximate expression for the exact nonlinear energy transfer integral, which includes only the two pairs of resonant wave components out of an infinite number of possible combinations.

The energy dissipation $S_{ds}$ is adopted from Komen *et al.* (1984), in which various $S_{ds}$ forms were tested with predetermined $S_{in}$ and $S_{nl}$, and the formula which gave the best agreement with the PM spectrum was adopted. The formula for $S_{ds}$ is given as

$$S_{ds} = -2.33 \times 10^{-5} \hat{\omega} (\omega / \hat{\omega})^2 (\hat{\alpha} / \hat{\alpha}_{PM})^2 F \ , \tag{2.32}$$

where $\hat{\omega} \equiv \left[ E^{-1} \int F(f,\theta) \omega \, df d\theta \right]^{-1}$ is the mean angular frequency and $\hat{\alpha} \equiv E \hat{\omega}^4 g^{-2}$ is a kind of nonlinear parameter.

A first-order forward upstream scheme is used in the calculation of energy propagation. Figure 2.8 shows examples of propagation of wave packets along various great circles. The distribution of propagated wave energy becomes broad, since the

forward upstream scheme has the property that computational diffusion becomes large. Especially in the case of propagation along latitude and longitude, computational diffusion in the direction of propagation becomes fairly large, so that the energy distribution becomes anisotropic.

The WAM model is adopted widely as an operational ocean wave prediction model in ECMWF, Bureau of Meteorology in Australia, etc. because of its high potential for ocean wave prediction. The accuracy of the model was verified by comparison with buoy and satellite data (*e.g.*, Zambresky, 1989; Romeiser, 1993). However, the model has some problems: the lack of accuracy in the energy propagation scheme, the use of the formula proportional to $u_*/c$ for $S_{in}$, whereas it can be considered to be proportional to $(u_*/c)^2$, the lack of accuracy in $S_{nl}$, and the lack of physical consideration in $S_{ds}$.

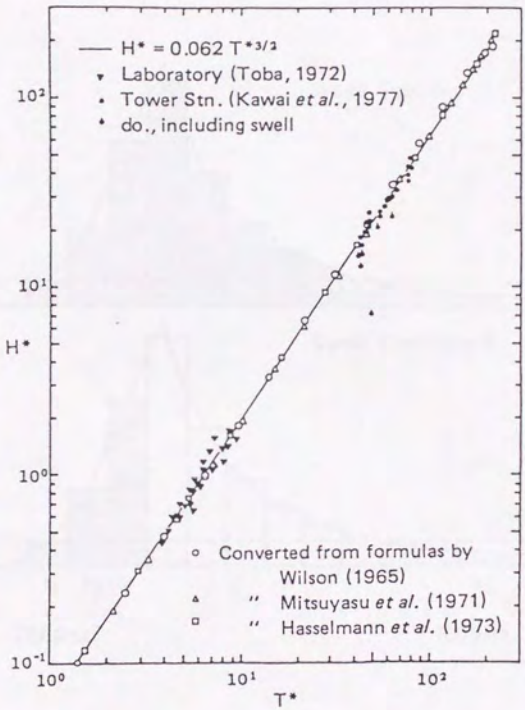


**Figure 2.6** The 3/2 power law between non-dimensional significant wave height and period with composed data (from Kawai *et al.*, 1977).

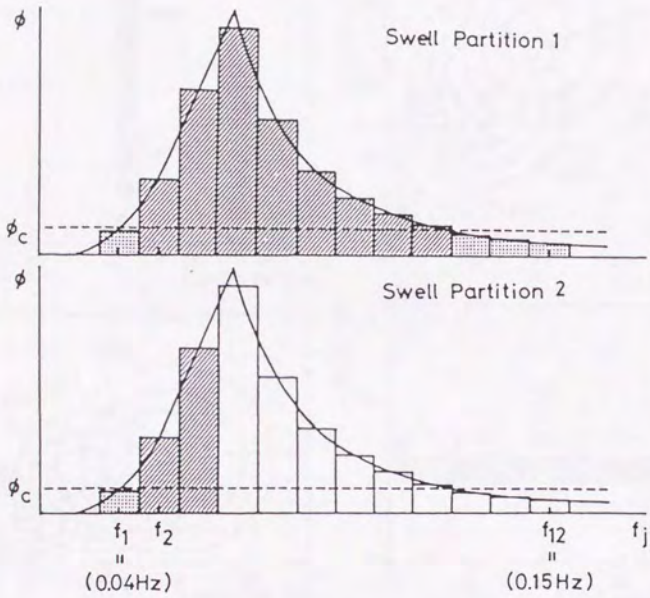


**Figure 2.7** A schematic illustration of swell partition 1 and partition 2 in the TOHOKU model. The area with dots and shade corresponds to the swell energy, and with shade only propagates as swell. The $\phi_c$ stands for cut off energy level (from Toba *et al.*, 1985).

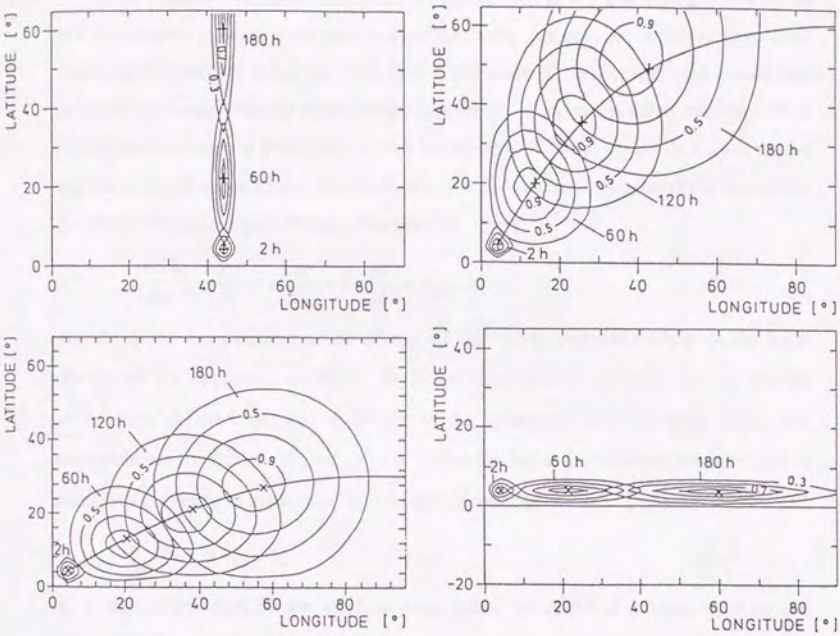


**Figure 2.8** Propagation of wave packets along various great circle paths for an initial $\delta$-function pulse with the first-order upstream propagation scheme. Contour lines are normalized against the maximum energy and its interval is 0.1. Teoretical propagation points are indicated by cross marks (from WAMDI Group, 1988).

## 3. The third generation ocean wave model JWA3G

### 3.1 Basic equations

If we assume that ocean waves can be represented as a linear superposition of an infinite number of wave components in which wave numbers are different from each other, the evolution of ocean waves in time $t$ and space $\boldsymbol{x}$ can be expressed as a change of wave spectrum $F(\boldsymbol{k};\boldsymbol{x},t)$ where wave number $\boldsymbol{k}$ is an independent variable. Here typical scales of time $t$ and space $\boldsymbol{x}$ must be regarded as larger values than wave period and wave length respectively. The evolution of wave spectrum is generally governed by the energy transport equation (*e.g.*, Hasselmann, 1968)

$$\frac{DF(\boldsymbol{k})}{Dt} \equiv \frac{\partial F}{\partial t} + \dot{\boldsymbol{x}} \cdot \frac{\partial F}{\partial \boldsymbol{x}} + \dot{\boldsymbol{k}} \cdot \frac{\partial F}{\partial \boldsymbol{k}} = S_{net} \ , \tag{3.1}$$

$DF/Dt$ is the Lagrangian rate of change of the wave spectrum. $\partial F/\partial t$ is the local change of the spectrum, $\dot{\boldsymbol{x}} \cdot \partial F/\partial \boldsymbol{x}$ is the change of the spectrum due to energy propagation in space $\boldsymbol{x}$, and $\dot{\boldsymbol{k}} \cdot \partial F/\partial \boldsymbol{k}$ is the refraction term. In deep water, the refraction term vanishes. $S_{net}$ of (3.1) is called the net energy source function and is expressed generally as the sum of three source functions:

$$S_{net} = S_{in} + S_{nl} + S_{ds} \ . \tag{3.2}$$

$S_{in}$ is the energy input by the wind. In some cases, the effect of adverse wind on the wave energy dissipation is included into $S_{in}$. $S_{nl}$ is the nonlinear energy transfer due to resonant wave-wave interactions by which the energy of each wave component is redistributed. The shape of the two-dimensional wave spectrum is changed due to the nonlinear energy transport, whereas the sum of the energy of all wave components remains unchanged. $S_{ds}$ is the energy dissipation due to wave breaking or bottom friction.

If all of the source functions are given in time and space, we can obtain the change of wave spectrum in time and space, by means of the numerical integration of equation (3.1), given a proper initial condition and boundary condition. However, the source functions are still not completely understood even considering the most recent studies.

Therefore it is necessary to express the source functions using empirical and approximate formulae based on observational and experimental results. There are many types of ocean wave models according to the expressions used for the source functions, the numerical treatment of equation (3.1) and whether shallow-water effects are considered or not.

The ocean wave model JWA3G which is developed in this study is a third generation wave model in the spherical coordinate system. To mention a few of the merits of the third generation wave model, one is the explicit calculation of the nonlinear energy transfer, using as many degrees of freedom as possible. The other is the use of no assumption on the existence of a fully-developed wave spectrum, while the first and second generation wave models were constructed on the assumption of the existence of a fully-developed wave spectrum. It was found that the third generation wave model gave a high accuracy of the calculated two-dimensional spectrum especially in the case of a suddenly-changing wind field (WAMDI Group, 1988).

The energy transport equation (3.1) for deep water, in spherical coordinates of latitude $\phi$ and longitude $\lambda$, is (*cf.* Appendix A)

$$\frac{\partial F}{\partial t} + \frac{1}{\cos\phi}\frac{\partial}{\partial\phi}\left(\dot{\phi}\cos\phi \cdot F\right) + \frac{\partial}{\partial\lambda}\left(\dot{\lambda}\cdot F\right) + \frac{\partial}{\partial\theta}\left(\dot{\theta}\cdot F\right) = S_{in} + S_{nl} + S_{ds} , \qquad (3.3)$$

where $F(f,\theta;\phi,\lambda,t)$ is the two-dimensional ocean wave spectrum, $f$ the frequency, $\theta$ the wave direction which is measured clockwise relative to true north and $t$ is time. $\dot{\phi}$, $\dot{\lambda}$ and $\dot{\theta}$ represent the rates of change of the position and propagation direction of a wave packet traveling along a great circle path (*cf.* Appendix B):

$$\dot{\phi} = \frac{d\phi}{dt} = \frac{C_g}{R}\cos\theta , \qquad (3.4)$$

$$\dot{\lambda} = \frac{d\lambda}{dt} = \frac{C_g}{R}\frac{\sin\theta}{\cos\phi} , \qquad (3.5)$$

$$\dot{\theta} = \frac{d\theta}{dt} = \frac{C_g}{R}\sin\theta \cdot \tan\phi . \qquad (3.6)$$

Here $g$ is the gravitational acceleration, $R \doteqdot 6371$km is the radius of the earth and $C_g = g/4\pi f$ is the group velocity.

### 3.2 Energy input by the wind $S_{in}$

With respect to the energy input by the wind, the Phillips-Miles combined mechanism

$$S_{in}(f,\theta) = A + B \cdot F(f,\theta) \ , \tag{3.7}$$

was proposed (Miles, 1960). The term $A$ corresponds to Phillips' (1957) resonance mechanism. This mechanism occurs when a component of the surface pressure distribution moves at the same speed as the free-surface wave with the same wave number. According to Phillips' mechanism, the energy transport equation can be approximated to $DF/Dt \approx A$, which results in the linear growth of wave energy in proportion to the time. It can be considered that Phillips' mechanism is ineffective as the growth mechanism of wind waves, but is effective as the trigger mechanism before Miles' mechanism.

The term $B \cdot F(f,\theta)$ in equation (3.7) corresponds to Miles' (1957) instability mechanism. When a parallel shear flow exists over the sea surface accompanied with an ocean wave, an instability of the air flow occurs in the critical layer where the mean wind speed is equal to the phase speed of the wind waves. The momentum of the mean wind is transferred downward due to the instability. The momentum transfer is proportional to the curvature of the wind profile at the critical layer. According to Miles' mechanism, the energy transport equation can be approximated to $DF/Dt \approx B \cdot F$, which results in the exponential growth of wave energy in time. Since the observed growth rate of wind waves was mostly an exponential function of time, it seemed that the growth of wind waves was explained by the theory. But it was found later that the growth rate expected from the theory was far smaller than the observed one (*e.g.*, Snyder and Cox, 1966; Barnett and Wilkerson, 1967), so that Miles' mechanism was shown to be ineffective as the growth mechanism. Recently, Miles (1993) modified Miles' (1957) theory. This time the wave-induced perturbations of the Reynolds stresses were considered, and the theory showed good agreement with the observed growth rate.

The Phillips-Miles combined mechanism was not successful in explaining theoretically the generation and growth of wind waves. However, many studies, in which empirical relations were found for the $A$ and $B$ terms, are performed by means of

wind-wave tunnel experiments or ocean wave observations (*e.g.*, Snyder *et al.*, 1981; Mitsuyasu and Honda, 1982; Hsiao and Shemdin, 1983).

As mentioned above, Phillips' mechanism mainly contributes to the generation of wind waves. Since the JWA3G model is expected to use the previously-calculated wave spectrum as an initial condition, Phillips' mechanism is excluded from the model by setting $A = 0$.

Figures 3.1 and 3.2 show experimental results and growth curves from many studies. Most of the experimental growth curves are proportional to $(u_*/c)^2$, where $u_*$ is the friction velocity of the air and $c$ is the phase speed of the wave component. The growth curve of Snyder *et al.* (1981), which was incorporated into the WAM model (WAMDI Group, 1988), is proportional to $u_*/c$. In JWA3G, considering the facts that most of the experimental relations are not proportional to $u_*/c$, but to $(u_*/c)^2$, a combined growth relation of Mitsuyasu and Honda (1982) and Hsiao and Shemdin (1983) is proposed:

$$B = \begin{cases} 0.065\left(\dfrac{u_*}{c} - 0.018\right)^2 \cdot 2\pi f\ , & \dfrac{u_*}{c} \le 0.2 \\ 0.34\left(\dfrac{u_*}{c}\right)^2 \cdot f\ . & \dfrac{u_*}{c} > 0.2 \end{cases} \tag{3.8}$$

In the range $u_*/c > 0.2$, a typical measurement range in wind-wave tunnel experiments, the growth rate of Mitsuyasu and Honda (1982) is adopted. On the other hand, in the range $u_*/c \le 0.2$, a typical measurement range for ocean wave observations, the growth rate of Hsiao and Shemdin (1983) is adopted, modifying its coefficient to maintain continuity at $u_*/c = 0.2$.

As shown in Figure 3.3, the growth curve (3.8) almost agrees with Snyder *et al.* (1981) in the range $u_*/c \le 0.1$, but in the range $u_*/c > 0.1$, the growth rate of Snyder *et al.* (1981) is far smaller than other growth rates. So the WAM model gives far smaller growth rate than the results of wind-wave tunnel experiments, if it is applied in the range $u_*/c > 0.1$.

We adopt the $\cos\theta$ distribution as the directional distribution of $S_{in}$ as follows:

$$S_{in} = B\cos(\theta_a - \theta_w) \cdot F(f, \theta)\ , \tag{3.9}$$

where $\theta_a$ and $\theta_w$ are the wind direction and wave direction, respectively. Energy dissipation due to adverse wind is expressed by putting a minus sign to the $B$ term of equation (3.8). The rationale for this idea is based on the experimental results (*e.g.*, Tsuruya, 1988; Mitsuyasu and Yoshida, 1989) in which the energy dissipation rate due to adverse wind was found to have nearly same magnitude as the growth rate of wind waves.

If we combine the ocean wave model with an atmospheric model, the friction velocity $u_*$ can be obtained through the atmospheric boundary layer model. But the wind speed at 10 m height $u_{10}$ is only available from observations or objective analysis. Therefore it is necessary to convert $u_{10}$ into $u_*$ by means of the drag relation

$$u_* = u_{10}\sqrt{C_D} \ . \tag{3.10}$$

Here, the drag coefficient $C_D$ should be expressed essentially as a non-dimensional value. Most relations for $C_D$ are expressed as a linear function of $u_{10}$ (*e.g.*, Garatt, 1977). We adopt the experimental relation by Wu (1980),

$$C_D = (0.8 + 0.065u_{10}) \times 10^{-3} \ . \tag{3.11}$$

Equation (3.11) is applicable to neutral conditions of atmospheric stability. It is known that the drag coefficient $C_D$ becomes greater than equation (3.11), as shown in Kondo (1975) under unstable conditions in which sea surface temperature is greater than atmospheric temperature.

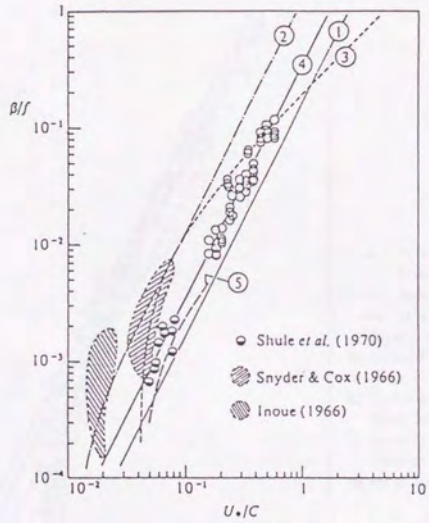


**Figure 3.1** Comparison of various experimental results for wind wave growth from Mitsuyasu and Honda (1982).
①:Miles(1959), ②:Inoue(1966), ③:Snyder and Cox(1966), ④:Mitsuyasu and Honda(1982), ⑤:Snyder *et al.*(1981).

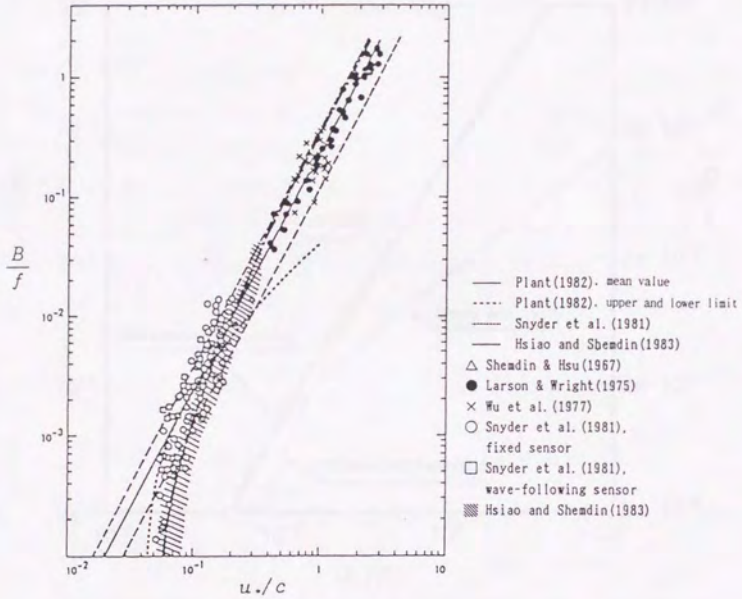


**Figure 3.2** Same as Figure 3.1, but from Hsiao and Shemdin (1983).

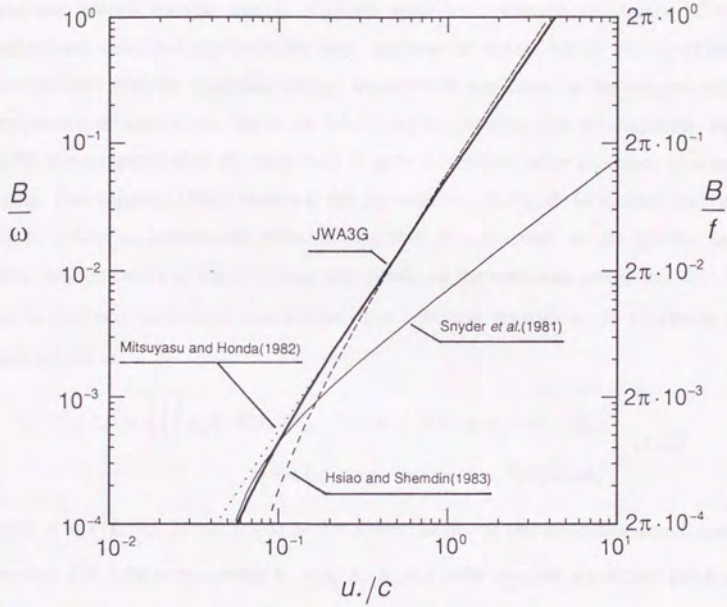


**Figure 3.3** Various growth curves for wind waves with the combined formula in the JWA3G model (thick line).

### 3.3 Nonlinear energy transfer $S_{nl}$

The spectral wave models using energy transport equations are based on the linear theory, in which it is assumed that the ocean wave field can be expressed as a linear superposition of an infinite number of wave components with random phases. However, nonlinear energy transfer due to resonant wave-wave interactions occurs, if the perturbation analysis is applied to the basic equations of surface waves. Phillips (1960) demonstrated that the nonlinear energy transfer did not occur in the second-order perturbation of wave slope, but in the third-order perturbation. But the magnitude was ineffective compared with the magnitude of growth and dissipation processes of ocean waves. Hasselmann (1962) extended the perturbation theory to fifth-order analysis which yielded a fourth-order effect comparable in magnitude to the growth and dissipation processes of ocean waves, and introduced the nonlinear energy transfer $S_{nl}$ due to resonant wave-wave interactions. The nonlinear transfer $S_{nl}$ is expressed in integral form as

$$\begin{aligned} S_{nl}(\boldsymbol{k}_4) = \iiint \omega_4 \sigma \cdot \delta(\boldsymbol{k}_1 + \boldsymbol{k}_2 - \boldsymbol{k}_3 - \boldsymbol{k}_4) \cdot \delta(\omega_1 + \omega_2 - \omega_3 - \omega_4) \\ \times \left[ n_1 n_2 (n_3 + n_4) - n_3 n_4 (n_1 + n_2) \right] d\boldsymbol{k}_1 d\boldsymbol{k}_2 d\boldsymbol{k}_3 , \end{aligned} \tag{3.12}$$

where $n_i = F(\boldsymbol{k}_i)/\omega_i, (i = 1, 2, 3, 4)$ is the action density of the two-dimensional wave spectrum $F(\boldsymbol{k}_i)$ for wave number $\boldsymbol{k}_i$, $\sigma(\boldsymbol{k}_1, \boldsymbol{k}_2, \boldsymbol{k}_3, \boldsymbol{k}_4)$ is the coupling coefficient and $\delta$ is the delta function representing the resonant conditions between four wave components:

$$\begin{cases} \boldsymbol{k}_1 + \boldsymbol{k}_2 = \boldsymbol{k}_3 + \boldsymbol{k}_4, \\ \omega_1 + \omega_2 = \omega_3 + \omega_4. \end{cases} \tag{3.13}$$

Figure 3.4 is the interaction chart from Hasselmann (1963). The interaction curves for different values of $\gamma \equiv \sqrt{k_1} + \sqrt{k_2} = \sqrt{k_3} + \sqrt{k_4}$, which is obtained by substituting the dispersion relation $\omega^2 = gk$ into the second equation of (3.13), are shown in the figure. The resonant condition between four wave components $(\boldsymbol{k}_1, \boldsymbol{k}_2, \boldsymbol{k}_3, \boldsymbol{k}_4)$ is given by the two pairs of wave number vectors of which end points $P$ and $P'$ lie on the same interaction curve. Since any set of $\gamma$, $P$ and $P'$ is available, it is easy to understand that there is an infinite number of combinations of wave components.

Equation (3.12) represents the rate of change of the wave energy of the $\boldsymbol{k}_4$ component in time, due to the resonant wave-wave interactions between the $(\boldsymbol{k}_1, \boldsymbol{k}_2, \boldsymbol{k}_3)$ components. When the two-dimensional wave spectrum is expressed in terms of discrete wave components, the integral operator in (3.12) is replaced by the summation of all the combinations of wave components. For example, in the JWA3G model, the two-dimensional spectrum is expressed by 900 wave components, so that the number of combination is $900^3 \approx 10^9$. Therefore it is almost impossible to incorporate the exact nonlinear calculations of $S_{nl}$ into a practical ocean wave model, even if using a supercomputer.

In order to reduce the amount of calculation, incorporation of the parameterized scheme into wave models, in which exact nonlinear energy transfer for a standard wave spectrum was parameterized by means of a few parameters, was attempted. Barnett (1968) parameterized the nonlinear energy transfer for the Neumann spectrum, and the Barnett's parameterized scheme was adopted by Yamaguchi *et al.* (1979). Young (1987) parameterized the nonlinear energy transfer for the JONSWAP spectrum and incorporated the scheme into an ocean wave model. But there was a limit to the range of sea states to which this parameterization could be applied, especially in the case of a bi-directional wave spectrum due to a sudden change of winds. The application of the parameterization scheme to that condition was difficult.

In order to solve the problem, Hasselmann *et al.* (1985) proposed a discrete interaction approximation which approximated the nonlinear energy transfer by means of an explicit calculation scheme. It was shown that the approximation, in which a certain limited number of combinations of the interacting wave components stood for the infinite number of combinations, could explain most of the nonlinear energy transfer. This discrete interaction approximation was adopted as the scheme for nonlinear energy transfer in the WAM model.

The comparison of the discrete interaction approximation with the exact calculation of $S_{nl}$ by Hasselmann and Hasselmann (1981) is shown in Figure 3.5. The four cases shown in the figure correspond to $\gamma = 1.0$ through $\gamma = 3.3$, where $\gamma$ is the peak enhancement coefficient of the JONSWAP spectrum. Since the treatment of

singular points in Hasselmann and Hasselmann (1981) is insufficient, the results of the exact calculation are not smooth (Masuda, 1980). In the case of $\gamma = 1.0$, which corresponds to the PM spectrum, the results calculated by the two different schemes almost agree. But the accuracy of the discrete interaction approximation becomes worse as the peak of the spectrum becomes sharp ($\gamma$ becomes larger), and in the case of $\gamma = 3.3$, the amount of the nonlinear energy transfer by the approximation is an order of magnitude smaller than that by the exact calculation. In the actual ocean wave field, it can be considered that a developed spectrum is gradually approaching a saturated PM spectrum ($\gamma = 1.0$), while in the generation and growth stage of wind waves, the peak of the spectrum is considered as more sharp than the PM spectrum, so that $\gamma$ is greater than 1. So the accuracy of the discrete interaction approximation by Hasselmann *et al.* (1985) is insufficient, especially in the case that $\gamma$ is greater than 1. The amount of nonlinear energy transfer is found to be significantly underestimated. In the JWA3G model, we have succeeded in improving the accuracy of the discrete interaction approximation by changing the combination of resonant wave components from the original pair of Hasselmann *et al.* (1985).

The improved discrete interaction approximation calculates the nonlinear energy transfer between resonant wave components of

$$\begin{cases} \omega_1 = \omega_2 = \omega, \\ \omega_3 = (1+\lambda)\omega = \omega_+, \\ \omega_4 = (1-\lambda)\omega = \omega_-, \end{cases} \tag{3.14}$$

with $\lambda = 0.19$, while $\lambda = 0.25$ was adopted in Hasselmann *et al.* (1985). From equation (3.14) and the first equation of (3.13), the wave directions of resonant wave components are found to be

$$\begin{cases} \theta_1 = \theta_2 = 0^\circ, \\ \theta_3 = \pm 10.20^\circ, \\ \theta_4 = \mp 22.47^\circ. \end{cases} \tag{3.15}$$

The improved discrete interaction approximation of the nonlinear energy transfer $S_{nl}$ is expressed as

$$\begin{Bmatrix} \delta S_{nl} \\ \delta S_{nl}^{+} \\ \delta S_{nl}^{-} \end{Bmatrix} = \begin{Bmatrix} -2\dfrac{\Delta f \Delta\theta}{\Delta f \Delta\theta} \\ (1+\lambda)\dfrac{\Delta f \Delta\theta}{\Delta f^{+} \Delta\theta} \\ (1-\lambda)\dfrac{\Delta f \Delta\theta}{\Delta f^{-} \Delta\theta} \end{Bmatrix} \tag{3.16}$$

$$\times C g^{-4} f^{11} \left\{ F^2 \left[ \frac{F_+}{(1+\lambda)^4} + \frac{F_-}{(1-\lambda)^4} \right] - 2\frac{F F_+ F_-}{\left(1-\lambda^2\right)^4} \right\} ,$$

where $\delta S_{nl}$ is the change of the nonlinear energy transfer per unit time, $F \equiv F(f,\theta)$ the two-dimensional wave spectrum, $\Delta f$ the frequency interval and $\Delta\theta$ is the angular interval. The increments $\Delta f \Delta\theta$ in the numerator refer to the "collision element", while those in the denominator refer to the element where the spectrum changes. The constant $C$ is a coupling coefficient which is chosen as $C = 2.5 \times 10^7$, for which the approximation agrees with the exact calculation.

Figure 3.6 shows a comparison of the improved discrete interaction approximation with the exact calculation by Hasselmann and Hasselmann (1981). The amount of the nonlinear energy transfer for the sharp spectrum of $\gamma > 1.0$ shows fair agreement with the exact calculation. It is found that for the sharp spectrum, the accuracy of the approximation with this scheme is much improved compared with Hasselmann's original approximation. According to Masuda (1986), it was shown that the nonlinear energy transfer for a broad spectrum such as the PM spectrum was not sensitive to the combination of resonant wave components, while that for a sharp spectrum was sensitive to the combination. For the case of $\lambda = 0.25$, since the difference in frequency of the resonant $\omega_+$ and $\omega_-$ components is rather larger than the half width of JONSWAP spectrum, the combination of resonant wave components of $\lambda = 0.25$ is inappropriate to express a principal part of the nonlinear energy transfer of the spectrum, while the components of $\lambda = 0.19$ can be considered as appropriate. Therefore the accuracy of the discrete interaction approximation with $\lambda = 0.19$ is improved.

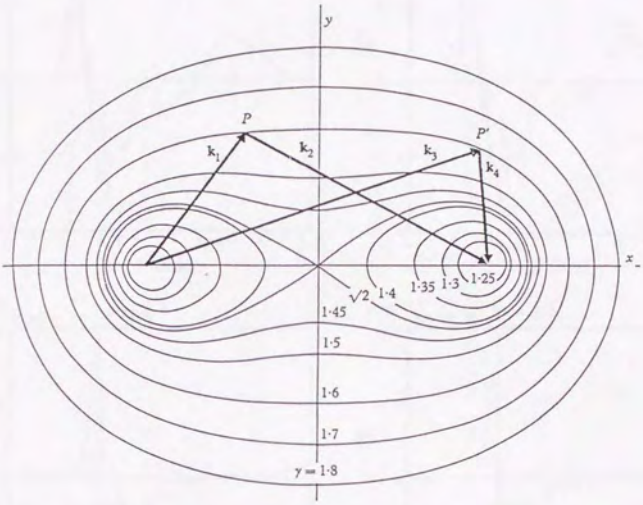


**Figure 3.4** Longuet-Higgins' interaction chart from Hasselmann (1963). Each contour line satisfies the resonant condition $\gamma \equiv \sqrt{k_1} + \sqrt{k_2} = \sqrt{k_3} + \sqrt{k_4}$, where $k_i$ is a wave number. The resonant condition of four wave components is expressed as two pairs of vectors on the same contour line of $\gamma$.

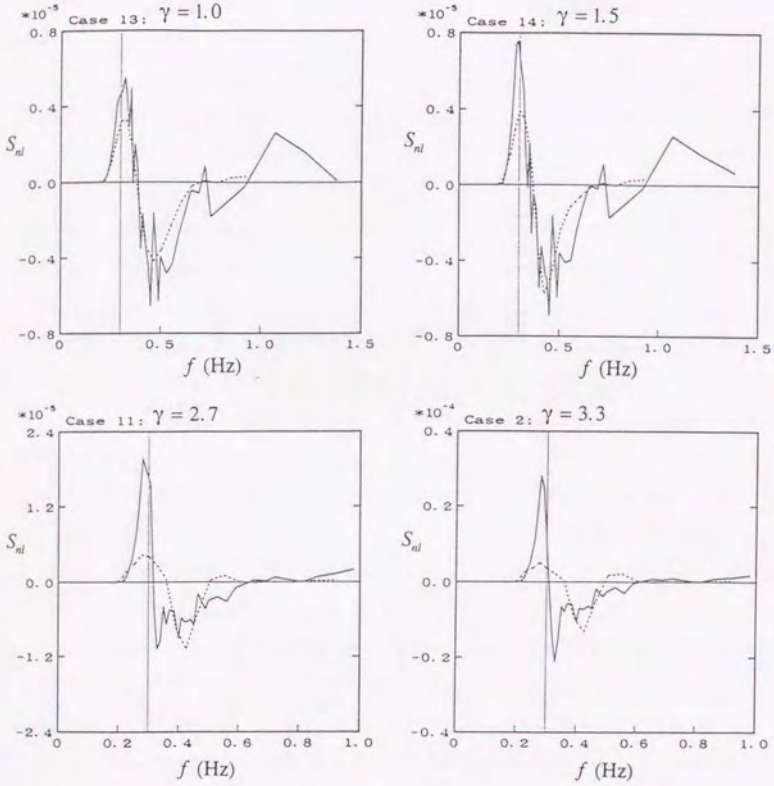


**Figure 3.5** The nonlinear energy transfer $S_{nl}$ for various wave spectra. Comparison of the results from Hasselmann *et al.* (1985) (dashed line) with the exact calculation by Hasselmann and Hasselmann (1981) (solid line). $\gamma$ is the peak enhancement coefficient of the JONSWAP spectrum.

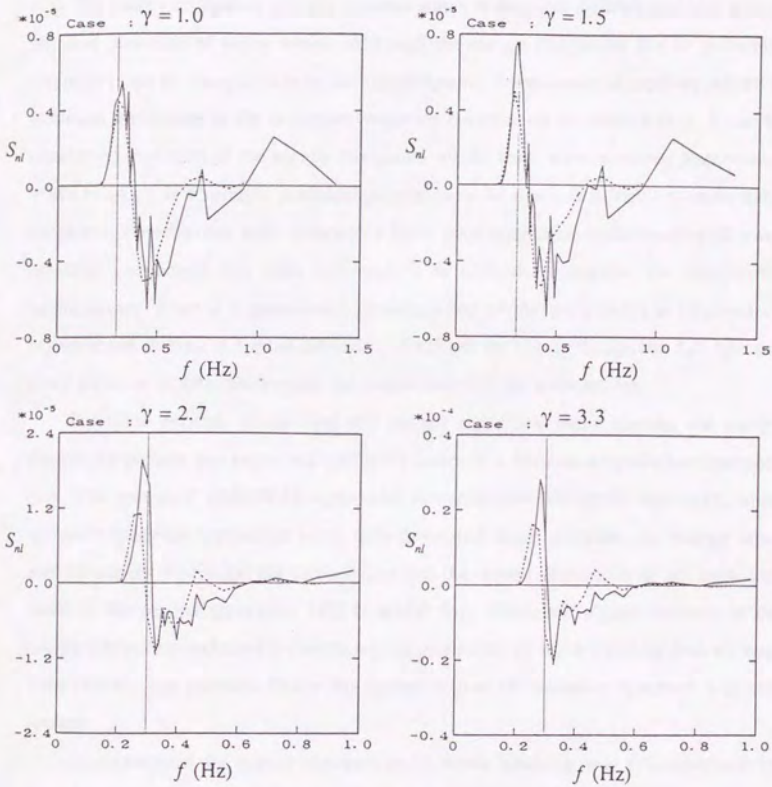


**Figure 3.6** Same as Figure 3.5, but for the improved discrete interaction approximation in the JWA3G model with $\lambda = 0.19$ (dashed line).

### 3.4 Energy dissipation $S_{ds}$

The energy dissipation process in ocean waves is the most difficult problem among physical processes of ocean waves. Although the energy dissipation due to molecular viscosity plays an essential role in the high-frequency components of capillary waves, it is almost ineffective in the dominant frequency components of ocean waves. It can be considered that most of the energy dissipation results from wave breaking phenomena. Wave breaking is a strongly nonlinear phenomenon, so that it is difficult to understand the physical mechanism well. Although a fairly good qualitative understanding of wave breaking phenomena has been achieved, it is difficult to express the mechanism quantitatively. Even if a quantitative understanding of the phenomena is obtained by experimental studies, it is quite difficult to distribute the energy dissipation into spectral components in order to incorporate the mechanism into the wave model.

For these reasons, in the first and second generation wave models, the energy dissipation process was expressed simply by means of a fully-developed wave spectrum (*e.g.*, PM spectrum; JONSWAP spectrum). According to this simple treatment, when the wave spectrum approaches some fully-developed wave spectrum, the energy input and the energy dissipation are balanced, so that the wave components do not grow any more. In the second generation MRI-II model (Uji, 1984), an original formula of the energy dissipation including the experimental probability of wave breaking derived from Toba (1979), was adopted. But in the model, a limit of saturation spectrum was still applied.

An expression for energy dissipation by wave breaking was first obtained by Hasselmann (1974). The expression, proportional to the second power of frequency, was obtained on the assumption that the effect of wave breaking was equivalent to that of the random pressure fluctuations in the air acting on the sea surface. For the purpose of incorporating the dissipation term into the wave model, Komen *et al.* (1984) obtained an expression for the energy dissipation by means of numerical simulation, in which the dissipation term was assumed to be proportional to the $n$th power of frequency and the $m$th power of a nonlinear parameter $\hat{\alpha} = E\overline{\omega^4}/g^2$, and the exponents $n$ and $m$ for which the simulation result gave good agreement with the PM spectrum were chosen as

$n = m = 2$. This gave the same result as Hasselmann (1974) that the energy dissipation is proportional to the second power of frequency. The expression obtained by Komen *et al.* (1984) is as follows:

$$S_{ds} = -3.33 \times 10^{-5} \overline{\omega} (\omega / \overline{\omega})^2 (\hat{\alpha} / \hat{\alpha}_{PM})^2 F, \tag{3.17}$$

where $\overline{\omega}$ is the first moment of angular frequency and $\hat{\alpha}_{PM} = 4.57 \times 10^{-3}$ is the theoretical value of $\hat{\alpha}$ for the PM spectrum. The expression (3.17) for the energy dissipation $S_{ds}$ is adopted in the WAM model (WAMDI Group, 1988).

In the JWA3G model, we propose an original formula for the energy dissipation based on the hypothesis of the source term balance and a scaling analysis. It is found that the exponents $n$ and $m$ in the Komen-type dissipation are determined analytically by the following considerations, while Komen *et al.* (1984) determined them by means of numerical simulations.

### 3.4.1 Energy balance between source terms

It is well known that the shape of the wind-wave spectrum has a self-similarity structure. It can be considered that the wind-wave spectrum in the high frequency range is inversely proportional to the 4th or 5th power of frequency (*e.g.*, Toba, 1973; Phillips, 1958). It is also considered that there is a local equilibrium between physical processes in wind waves in the high-frequency range (*e.g.*, Toba, 1972; Masuda and Kusaba, 1987), so that the wind-wave spectrum has a self-similarity structure. Phillips (1985) assumed an energy balance between source terms: the energy input by the wind $S_{in}$, the nonlinear energy transfer $S_{nl}$ and the energy dissipation $S_{ds}$, in the equilibrium range of the wind-wave spectrum. On the assumption that

$$S_{in} + S_{nl} + S_{ds} = 0, \tag{3.18}$$

Phillips (1985) introduced results that the wind-wave spectrum in the equilibrium range was proportional to $\omega^{-4}$, and the energy dissipation was expressed as $S_{ds} \propto gk^{-4}$, where $\omega$ is the angular frequency, $g$ the gravitational acceleration and $k$ is the wave number.

We start to develop a theory from the Phillips hypothesis (3.18) and assume furthermore that the magnitudes of each of the physical processes have the same order in

the equilibrium range:

$$S_{in} \approx S_{nl} \approx S_{ds} \ . \tag{3.19}$$

It is considered that both gravitational acceleration $g$ and friction velocity $u_*$ are essential as forcing terms in the process governing the growth of wind waves. Therefore $S_{in}$ and $S_{nl}$ are scaled in terms of $g$ and $u_*$ as (see Appendix C for the scaling of $S_{nl}$)

$$S_{in} \approx (u_*/c)^2 \omega F \approx g^{-2} u_*^2 \omega^3 F, \tag{3.20}$$

$$S_{nl} \approx g^{-4} \omega^{11} F^3, \tag{3.21}$$

where $c$ is the phase speed of the wind wave and $F$ is the wave spectrum. Substituting equations (3.20) and (3.21) into (3.19), we arrive at the following two conclusions:

a) The wind-wave spectrum $F(\omega)$ in the equilibrium range is proportional to $\omega^{-4}$:

$$F(\omega) \approx g u_* \omega^{-4}. \tag{3.22}$$

b) The energy dissipation $S_{ds}$ is proportional to $\omega^3$:

$$S_{ds} \approx g^{-2} u_*^2 \omega^3 F \ . \tag{3.23}$$

The conclusion that the wave spectrum in the equilibrium range is proportional to $\omega^{-4}$, which is derived from the assumptions, agrees well with the observed wind-wave spectra (*e.g.*, Kawai et al., 1977). Applying the same scaling analysis as mentioned above to the WAM model, in which the energy input $S_{in}$ proportional to $u_*/c$ is adopted, an energy dissipation proportional to $\omega^2$ is required from the balance between $S_{in}$ and $S_{nl}$. In fact, the energy dissipation of equation (3.17) in the WAM model is proportional to $\omega^2$, which is consistent with the result based on the energy balance hypothesis. It is also concluded that the wave spectrum in the equilibrium range is proportional to $\omega^{-4.5}$. Therefore the basic framework of physical processes in the WAM model is not supported by the local equilibrium hypothesis of wind waves, which is typically represented by Toba's (1972) 3/2 power law relating wave height and period.

### 3.4.2 The formula for energy dissipation

By considering the energy balance between source terms, we can obtain the dependence of the energy dissipation $S_{ds}$ on frequency as in equation (3.23). Then the formula for $S_{ds}$ is determined by means of dimensional analysis. We propose an

expression

$$S_{ds} = -C_b \overline{\omega} \left( \frac{\omega}{\overline{\omega}} \right)^3 \left( \frac{E^*}{E^*_{PM}} \right)^m F \ , \tag{3.24}$$

where,

$$\overline{\omega} = E^{-1} \iint \omega F(\omega, \theta)\, d\omega\, d\theta \quad , \tag{3.25}$$

$$E = \iint F(\omega, \theta)\, d\omega\, d\theta \quad , \tag{3.26}$$

and $E^* = \overline{\omega^4} / g^2 \cdot E$ is a nonlinear parameter which is proportional to the second power of the wave slope. $E^*_{PM} = 4.57 \times 10^{-3}$ is the theoretical value of $E^*$ for the PM spectrum. Komen *et al.* (1984) determined the exponent $m$ in equation (3.24) by means of several numerical experiments. However, it is found to be determined analytically by the following considerations on the condition to realize the 3/2 power law.

The 3/2 power law (Toba, 1972) between wave height and period is

$$H^* = B \cdot \left( T^* \right)^{3/2} \ , \tag{3.27}$$

where $H^* = g u_*^{-2} H$ is the non-dimensional significant wave height, $T^* = g u_*^{-1} T$ is the non-dimensional wave period and the constant $B = 6.2 \times 10^{-2}$ was determined from ocean wave observations. Toba (1973) showed that the wave spectrum that is consistent with the 3/2 power law in the equilibrium range was $g u_* \omega^{-4}$, which is the same formula as equation (3.22). By using $H^*$ and $T^*$, the wave energy $E$ and the mean angular frequency $\overline{\omega}$ are expressed as

$$E = \frac{1}{16} H^2 = \frac{1}{16} \left( g^{-1} u_*^2 H^* \right)^2 \ , \tag{3.28}$$

$$\overline{\omega} = 2\pi / T = 2\pi g u_*^{-1} / T^* \ . \tag{3.29}$$

Substituting equations (3.28) and (3.29) into (3.24) yields

$$S_{ds} \approx -g^{-2} u_*^2 \omega^3 \frac{\left( H^* \right)^{2m}}{\left( T^* \right)^{4m-2}} F \ . \tag{3.30}$$

Supposing that the energy dissipation $S_{ds}$ does not depend on the wave height and period, the exponent $m$ is determined as $m = 2$ by substituting the 3/2 power law (3.27) into

(3.30). The conclusion that $m = 2$ agrees with equation (3.17). The formula for $S_{ds}$ can be obtained by incorporating the experimental wind-wave relations skillfully into the model.

From the above considerations, although the original meaning of a third generation wave model was that the model should have no restriction on the growing wave spectrum, it becomes clear that the framework based on the experimental 3/2 power law is included implicitly not only in JWA3G but also in WAM.

The dissipation coefficient $C_b = 6.0 \times 10^{-5}$ is chosen so that the wind-wave growth under a constant wind field agrees with the experimental results. This coefficient $C_b$ plays a role in adjusting the wave model in total. This value is appropriate for calculations on a 2.5 degree grid interval. However, for other grid intervals, it will be necessary to re-examine the value of $C_b$, because the contribution from subgrid-scale phenomena (typhoons, fronts, etc.) varies. There are always these kinds of problems in modeling natural phenomena - this is known as the problem of eddy viscosity.

### 3.5 Finite difference scheme for energy propagation

The upstream finite difference scheme is the most suitable for calculating a propagation term of a positive-definite quantity such as a wave energy, because the centered scheme generates a negative energy. The forward upstream scheme is implemented in the WAM model. However there are some problems, in that the scheme generates a large computational diffusion, and the propagated energy distribution in spherical coordinates becomes anisotropic when the wave packet propagates along latitude or longitude directions (Figure 2.8). Therefore we have developed the following higher-order upstream scheme (Hybrid Upstream) in order to improve the accuracy. For the one-dimensional advection equation

$$\frac{\partial u}{\partial t} + c\frac{\partial u}{\partial x} = 0 , \tag{3.31}$$

if the advection speed $c > 0$, the Hybrid Upstream scheme is expressed as

$$\begin{cases} \dfrac{u_j^* - u_j^n}{\Delta t} + c\dfrac{u_j^n - u_{j-1}^n}{\Delta x} = 0 , \\ \dfrac{u_j^{n+1} - u_j^n}{\Delta t} + \dfrac{1}{\alpha+\beta}\left(\alpha c\dfrac{2u_{j+1}^n + 3u_j^n - 6u_{j-1}^n + u_{j-2}^n}{6\Delta x} + \beta c\dfrac{2u_{j+1}^* + 3u_j^* - 6u_{j-1}^* + u_{j-2}^*}{6\Delta x}\right) = 0 , \end{cases} \tag{3.32}$$

where $x = j\Delta x$, $t = n\Delta t$ and $\alpha = \beta = 1/2$ are the constants. The Hybrid Upstream scheme uses two-step calculations. The first equation of (3.32) is a predictor and the second equation is a corrector. The scheme adopts a forward upstream scheme as a predictor and a combination of third-order upstream schemes as a corrector. The scheme is conditionally stable with $c\,\Delta t/\Delta x \le 1$. There is a more highly-accurate scheme by Hsu and Arakawa (1990), than the Hybrid Upstream scheme, but the calculation procedure is so complicated that it is difficult to incorporate the scheme into a practical wave model.

A comparison of the Hybrid Upstream scheme with the forward upstream scheme for the one-dimensional advection equation is shown in Figure 3.7. The shape of the propagated energy distribution is almost preserved in the Hybrid Upstream scheme, while the shape is not preserved in the forward upstream scheme. In the latter, the energy peak becomes smaller and its distribution becomes broad due to the computational diffusion. So it is clear that Hybrid Upstream scheme is a highly-accurate

one.

### 3.5.1 Stability analysis

The von Neumann stability analysis is applied to the Hybrid Upstream scheme for determining the stability condition. In the von Neumann method, the solutions of equation (3.32) are expanded as a finite Fourier series, in which a Fourier component is expressed as

$$u_j^n = U^n \exp\left[ik(j\Delta x)\right], \tag{3.33}$$

where $n$ denotes an index of time $t = n\Delta t$ and $j$ denotes that of space $x = j\Delta x$. Substituting equation (3.33) into (3.32), the amplification factor $G \equiv U^{n+1}/U^n$ is given as

$$\begin{aligned} G = &\left(-\frac{\mu}{3} + \frac{\beta}{\alpha+\beta}\frac{\mu^2}{3}\right)e^{ik\Delta x} + 1 - \frac{\mu}{2} + \frac{\beta}{\alpha+\beta}\frac{\mu^2}{6} + \left(\mu - \frac{\beta}{\alpha+\beta}\frac{3\mu^2}{2}\right)e^{-ik\Delta x} \\ &+ \left(-\frac{\mu}{6} + \frac{\beta}{\alpha+\beta}\frac{7\mu^2}{6}\right)e^{-2ik\Delta x} - \frac{\beta}{\alpha+\beta}\frac{\mu^2}{6}e^{-3ik\Delta x}, \end{aligned} \tag{3.34}$$

where $\mu \equiv c\,\Delta t/\Delta x$. The general stability requirement is $|G| \le 1$ for any $k\Delta x$. Figure 3.8 shows the real and imaginary components of $G$ for various $\mu$ values and Figure 3.9 shows the absolute values $|G|$ for various $\mu$ values. It is found that the amplification factor $|G|$ never exceeds 1.0 under the condition of $\mu \le 1.0$. But in the range of $0.5 < \mu \le 1.0$, $|G|$ takes a minimum value at a certain wave length (Figure 3.9), where the rapid change of the real and imaginary parts of $G$ (Figure 3.8) indicates the rapid phase change of the solution. Thus, it is desirable to apply the Hybrid Upstream scheme with $\mu \le 0.5$.

### 3.5.2 Artificial diffusion

It is true that a highly-accurate finite difference scheme is generally desirable, but in the case of energy propagation in ocean wave models, in which the directional spectrum is discretized in frequency and direction, highly-accurate schemes do not always give the best results. Figure 3.10 shows a schematic figure of the propagation of a wave packet initially concentrated at the origin (SWAMP Group, 1985). If the wave packets propagate without any diffusion, spectral bins represented by rectangular

regions keep their sizes. However, the area where no wave packet arrivals increases as the wave packets propagate far from the origin. This problem comes from the discretization of the directional spectrum into finite wave number components. In reality, the wave spectrum is continuous in both frequency and direction so that the propagated energy distribution should cover the whole space continuously. In the old wave models, this kind of problem was not noticeable, because energy propagation schemes with high computational diffusion such as the jumped method (Isozaki and Uji, 1973) or the forward upstream scheme (WAMDI Group, 1988) were implemented in the models. On the other hand, in the JWA3G model, since a highly-accurate finite difference scheme is adopted, it becomes a problem to keep the continuity of the propagated energy distribution.

Therefore an artificial diffusion term is added to the energy propagation scheme so as to realize an idealized energy propagation. The energy transport equation with the artificial diffusion term is expressed as

$$\frac{\partial F}{\partial t}+\frac{1}{\cos\phi}\frac{\partial}{\partial\phi}\left(\dot{\phi}\cos\phi\cdot F\right)+\frac{\partial}{\partial\lambda}\left(\dot{\lambda}F\right)+\frac{\partial}{\partial\theta}\left(\dot{\theta}F\right) = S_{nel}+K_{\phi}\frac{\partial^2 F}{\partial\phi^2}+K_{\lambda}\frac{\partial^2 F}{\partial\lambda^2}\ , \tag{3.35}$$

where the diffusion coefficients $K_{\phi}$ and $K_{\lambda}$ are determined by the energy propagation test for the monotonic wave component:

$$\begin{cases} K_{\phi}=0.04\Delta\theta^2\left|\dfrac{C_g}{R}\dfrac{\sin\theta}{\cos\phi}\right|, \\ K_{\lambda}=0.04\Delta\theta^2\left|\dfrac{C_g}{R}\dfrac{\cos\theta}{\cos^2\phi}\right|. \end{cases} \tag{3.36}$$

Figure 3.11 shows an example of the energy propagation on a sphere. As shown in the figure, a wave packet is propagating along a great circle path and gradually changing its propagation direction. The reason is that there is a term which produces a change in propagation direction of a wave packet in the energy transport equation (3.3), which is characteristic of a propagation term in the spherical coordinate system. Propagation of wave packets along various great circle paths is shown in Figure 3.12, which is drawn after Figure 2.8 of WAMDI Group (1988). It is found that the computational diffusion

of JWA3G is much smaller than in WAM. In the case that wave packets are propagating along latitude or longitude directions, the propagated energy distribution of WAM is anisotropic, while that of JWA3G is not. Therefore the Hybrid Upstream scheme in JWA3G is considered as highly accurate and appropriate to the calculation of energy propagation in the wave model.

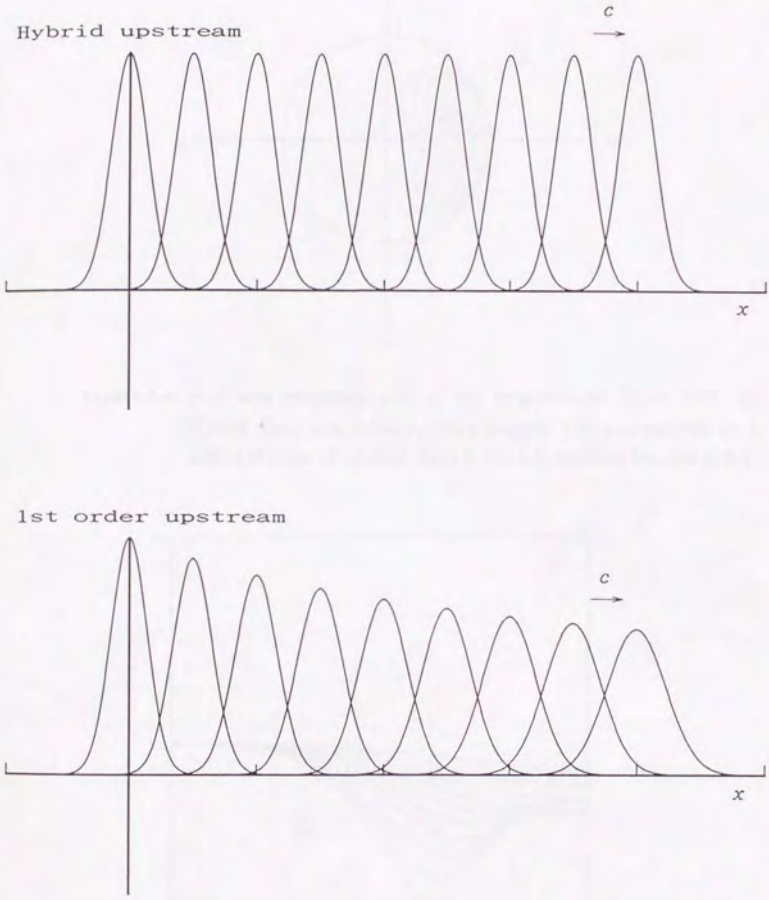


**Figure 3.7** The results of energy propagation by the Hybrid Upstream scheme (upper) and the first-order forward upstream scheme (lower). The condition $c\Delta t/\Delta x$ is 0.2. The result is plotted every 250 time steps.

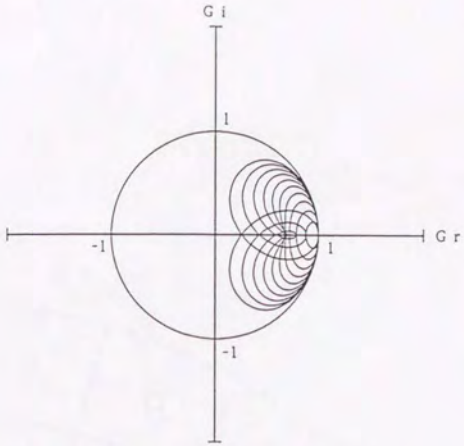


**Figure 3.8** Real and imaginary part of the amplification factor $G$ of the Hybrid Upstream scheme. Each contour line corresponds to a different value of $c\Delta t/\Delta x$ from 0.1 to 1.0. Contour interval is 0.1.

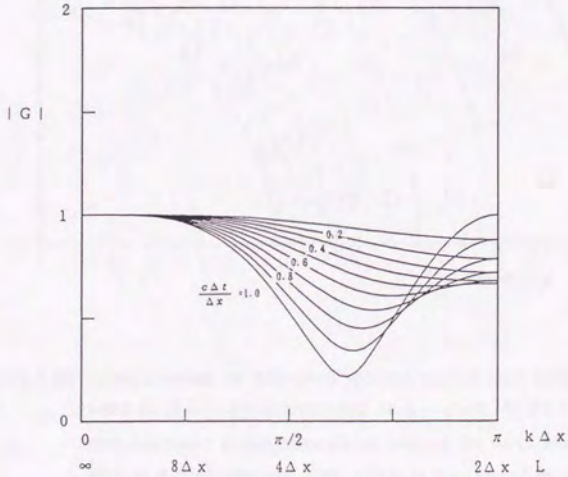


**Figure 3.9** The absolute amplification factor $|G|$ of the Hybrid Upstream scheme. Each contour line corresponds to a different value of $c\Delta t/\Delta x$ from 0.1 to 1.0. Contour interval is 0.1.

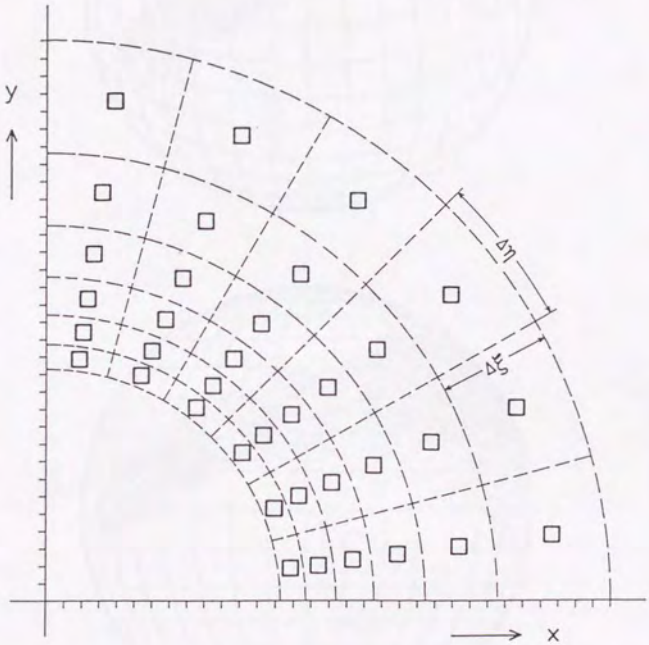


**Figure 3.10** Areas covered by individual spectral bins at each time for a wave field initially concentrated at $x = y = 0$. In the case of non-dispersive propagation (solid boxes), the wave energy is zero in the intermediate area, while in the case of dispersive propagation, the consistency requirements for propagation are satisfied (from SWAMP Group, 1985).

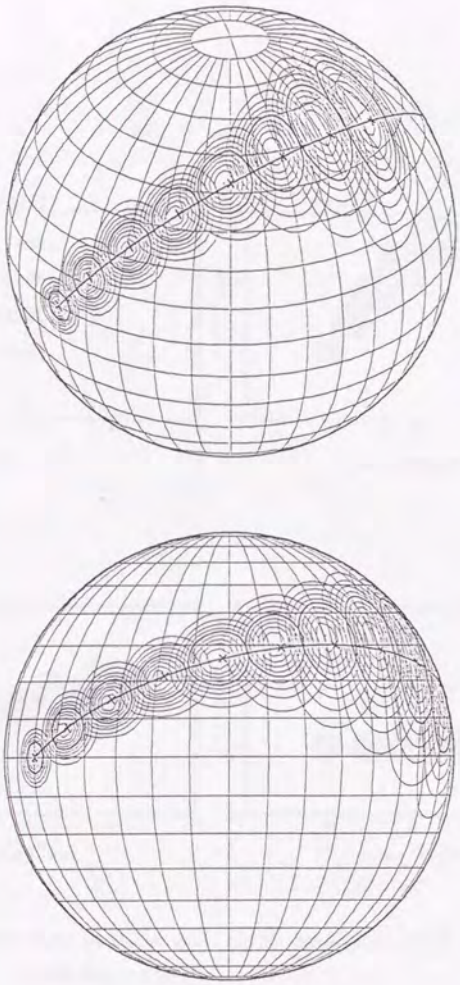

**Figure 3.11** An example of wave energy propagation by the Hybrid Upstream scheme on a sphere. Propagated energy is plotted at 60 hour intervals. Contour lines are normalized against the maximum energy and the contour interval is 0.1. Theoretical propagation points are indicated by cross marks.

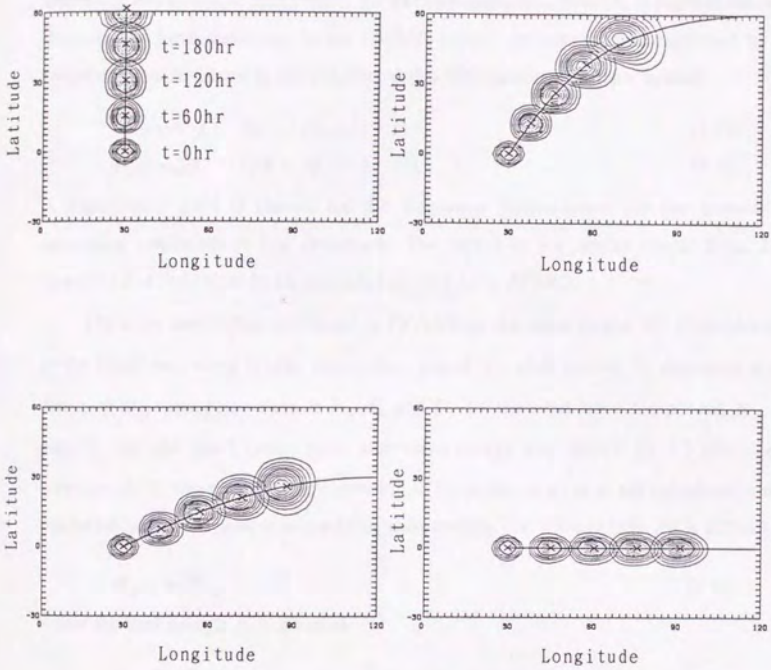


**Figure 3.12** Same as Figure 3.11, but for propagation along various great circle paths.

### 3.6 Definition of wave components and parameters

The evolution of the two-dimensional wave spectrum is calculated by means of the numerical integration of the energy transport equation. It is necessary to discretize the frequency and direction into a finite number of components in order to express the two-dimensional wave spectrum. In the JWA3G model, the spectrum is expressed by 25 frequency and 36 direction components, that is 900 wave components in total:

$$f_n = \alpha^{n-1} f_1 , \quad (\alpha = 1.09, \mathrm{n}=1\sim25) \tag{3.37}$$

$$\theta_n = n\Delta\theta . \quad (\Delta\theta = 10^\circ, \mathrm{n}=1\sim36) \tag{3.38}$$

A logarithmic scale is chosen for the frequency discretization for the purpose of increasing resolution in low frequency. The period in the model ranges from 28.6 seconds ($f_1 = 0.035\mathrm{Hz}$) to 3.6 seconds ($f_{max} = f_{25} = 0.277\mathrm{Hz}$).

The wave parameters calculated in JWA3G are the wave height $H_S$ corresponding to the significant wave height, momentum period $T_S$, peak period $T_P$, dominant wave direction $D_S$, wave parameters of $H_W$, $T_W$ and $D_W$ for the wind-wave component, $H_L$, $T_L$ and $D_L$ for the swell component, and wave energy and period for 12 directional components. A wave period corresponding to a significant wave is not calculated, but it can be related to the peak or momentum wave period. The wave height $H_S$ is defined as

$$H_S = 4\sqrt{E} , \tag{3.39}$$

where the total energy $E$ is given as

$$E = \sum_j \sum_i F(f_i, \theta_j)\Delta f_i \, \Delta\theta_j + \frac{1}{3}\sum_j F(f_{max}, \theta_j)\Delta\theta_j \cdot f_{max} . \tag{3.40}$$

The second term on the right side of equation (3.40) is the contribution from a tail spectrum, where it is assumed that the $f^{-4}$ spectrum continues beyond the highest frequency limit $f_{max}$. In the same way of using a tail contribution, the momentum wave period $T_S$ is defined as

$$T_S = 1\Big/\sqrt{\overline{f^2}} , \tag{3.41}$$

where the second moment of frequency is given as

$$\overline{f^2} = \frac{1}{E}\left[\sum_j \sum_i F(f_i, \theta_j) f_i^2 \Delta f_i \, \Delta\theta_j + \sum_j F(f_{max}, \theta_j) \Delta\theta_j \cdot f_{max}^3\right]. \qquad (3.42)$$

The dominant wave direction $D_S$ is defined as the direction in which the total wave energy is greatest. The peak period $T_P$ is defined as the period where the spectral energy is maximum.

It can be considered that there are many cases where the separation of swell and wind wave components is difficult. We refer to the separation method in the TOHOKU model, since CH models are based on the separate treatment of swell and wind-wave components. The separation in TOHOKU is that all wave components for which the difference between wind direction and wave direction is greater than $90^\circ$ are considered as swell components. When the difference between wind direction and wave direction is smaller than $60^\circ$ and the condition $c/u_{10} \leq 1.37$ is satisfied, the swell component is re-transformed into a wind-wave component. In JWA3G, which is classified as a CD model, swell and wind-wave components are not separated explicitly, so a simpler separation method is adopted. In this method, wind-wave components are defined as those which satisfy the inequality

$$f > 0.5 f_{PM} = 0.5 \frac{0.13g}{u_{10} \cdot \cos(\theta_w - \theta_a)}, \quad (\theta_w - \theta_a \leq 90^\circ) \qquad (3.43)$$

where $\theta_w$ is the wave direction and $\theta_a$ is the wind direction. The components which do not satisfy the inequality (3.43) are defined as swell. The separation is based on the assumption that the wind waves corresponding to the peak frequency of the PM spectrum are developing according to the wind speed. The criterion $c/u_{10} = 1.37$ in TOHOKU can be converted into $f = 0.116\, g/u_{10}$, so the criterion of (3.43) means that the threshold of wind waves is shifted toward a longer period range than that of TOHOKU. By introducing this criterion, separate wave parameters for swell and wind components are available, although they were not available in old wave models. Wave parameters of wave height, peak period and dominant direction are calculated for both swell and wind wave components.

The wave energy and period of 12 directional components are designed to be used instead of the two-dimensional wave spectrum. The amount of spectral information

from all grid points is so numerous that it is difficult to store the all spectra. By using 12 directional components, the amount of spectral information can be reduced. The energies of 12 directional components are stored as the equivalent wave heights in terms of equation (3.39).

### 3.7 Basic characteristics of the JWA3G model

In order to study the basic characteristics of the JWA3G model, the evolution of the ocean wave field was tested under uniform wind conditions. We focused on the subject of the evolution of the wave spectrum and the energy balance between each of the energy source functions. According to the hypothesis on the energy balance of each source function in the equilibrium range, the wave spectrum should be proportional to $f^{-4}$.

The evolution of waves is calculated in a rectangular sea within 60 degrees (about 6670 km), of which the center is located on the equator. A stationary, homogeneous wind field with wind speed $u_{10} = 20$ m/s blows perpendicularly offshore. The initial wave energy at time $t = 0$ is zero, and the wave spectrum at the upstream boundary remains zero for $t > 0$. The wave energy at the downstream boundary penetrates through the boundary. Fetch-limited growth of wave energy is observed at a point 55 degrees (about 6120 km) down-wind, which corresponds to the non-dimensional fetch $x^* = 7.1 \times 10^7$ after SWAMP Group (1985). The model is integrated over 500 hours, and the time step is $\Delta t = 30$ minutes.

Figures 3.13 and 3.14 show the evolution of the wave spectrum. The spectrum in Figure 3.14 is non-dimensionalized by means of division by $gu_* f^{-4}$. The spectrum is growing in proportion to $f^{-4}$, keeping its self-similarity structure. The fact that the spectral shape in the equilibrium range is proportional to $f^{-4}$ comes from the hypothesis on the energy balance between source functions. As is evident from Figure 3.14, in the initial development stage of the equilibrium spectrum, the overshoot phenomena, which were found by Barnett and Sutherland (1968), can be seen. It can be considered that the phenomena occur due to the effect of the nonlinear energy transfer $S_{nl}$.

The directional distribution functions at $t = 480$ hours are shown in Figure 3.15. The distribution near the spectral peak corresponds to $S = 8$ of Mitsuyasu's directional distribution function $\cos^{2S}(\theta/2)$. The distribution in the higher frequency range above the peak frequency becomes more broad than that at the peak. Mitsuyasu *et al.* (1975) gave results from ocean wave observations using a cloverleaf buoy showing that the energy concentration of the ocean wave spectrum was greatest near the spectral peak,

while it became smaller in both lower and higher frequency ranges. The directional distribution of wave energy in JWA3G almost agrees with the result from Mitsuyasu *et al.* (1975). But a slight difference between the model and observations is found in the lower frequency range, where the observational results show that the directional distribution is more broad than that of the spectral peak, while that in the model is not. For frequencies lower than $f_6$, which are not shown in Figure 3.15, the directional distribution becomes double-peaked in shape. It is considered that this result is due to the approximate scheme for the nonlinear energy transfer $S_{nl}$. Since the improved discrete interaction approximation expresses $S_{nl}$ in terms of only the symmetrical two pairs of resonant wave components, between which the differences in direction are restricted to between $10^\circ$ and $20^\circ$, the directional distribution becomes double-peaked in shape. Therefore it can be hoped that this problem will be solved and the distribution of the model becomes closer to those of the observations, as the approximation of $S_{nl}$ becomes more accurate by means of increasing the number of combinations of the resonant wave components.

Figures 3.16 and 3.17 show the non-dimensional energy source functions at $t = 480$ hours. The net source function $S_{net}$ still remains to develop the wave spectrum, which indicates that JWA3G has no asymptotic equilibrium spectrum. The spectral shape of the model is more sharp than the PM spectrum and its peak enhancement coefficient $\gamma$ is about 1.5.

The role of the energy source functions are as follows. Most of the energy input occurs at higher frequencies range than the spectral peak, and the obtained energy is transported toward lower frequencies by the nonlinear energy transfer $S_{nl}$. The energy input by the wind $S_{in}$ is roughly balanced with the energy dissipation $S_{ds}$ and these effects by themselves almost compensate each other. With respect to the directional distribution of the nonlinear energy transfer $S_{nl}$, as shown in Figure 3.17, the wave energy is transported from the high frequency range to the low frequency range in the case of $\theta = 0^\circ$, while being transported in the opposite direction in case of $\theta = 60^\circ$, so that the nonlinear energy transfer $S_{nl}$ has the effect of broadening the directional distribution in the high frequency range.

The energy balances of source functions by Komen *et al.* (1984) which correspond to Figure 3.17 are shown in Figure 3.18. The spectra at $x^* = 1.2 \times 10^8$ with $u_{10} = 15$ m/s are shown in the figure. The peak energy of the wave spectrum has nearly the same magnitude as that of JWA3G, however, the shape of the spectrum of the JWA3G model is more sharp than that of Komen *et al.* (1984). The magnitude of the energy input $S_{in}$ is three times larger than that of the JWA3G model, and the peak of $S_{in}$ is located at a higher frequency, so that the position of the peak of the two-dimensional wave spectrum is also shifted toward higher frequency. It can be considered that the differences arise from the effect of $S_{in}$, which is proportional to $(u_*/c)^2$ in JWA3G, while the formula of Snyder *et al.* (1981) proportional to $u_*/c$ is adopted in Komen *et al.* (1984). With respect to the nonlinear energy transfer $S_{nl}$, the energy distribution of Komen *et al.* (1984), in which the exact calculation scheme of $S_{nl}$ is adopted, shows a similar tendency to the result of the improved discrete interaction approximation in JWA3G. Therefore the improved discrete interaction approximation in JWA3G is found to be accurate enough for practical usage.

The comparison of JWA3G with other wave models is investigated by means of the SWAMP experiment, in which the precise conditions of calculation area and wind speed etc. are defined for 7 experiments named Cases Ⅰ-Ⅶ. Case Ⅱ aims at revealing some fundamental differences between wave models. In the Case Ⅱ experiment, the evolution of the wave field is investigated in a rectangular sea of 1125km with a stationary homogeneous wind speed $u_{10} = 20$ m/s. The drag coefficient is defined as $C_D = 1.83 \times 10^{-3}$ in order to produce the same friction velocity $u_*$. The fetch-limited test is the experiment in which the non-dimensional wave energy $E^*$ and the non-dimensional peak frequency $f_p^*$ are investigated as functions of the leeward fetch, when the wave field approaches a nearly fully-developed state. The duration-limited test is the experiment in which $E^*$ and $f_p^*$ at a fixed point on the leeward side are investigated as functions of integration time.

Figure 3.19 and 3.20 show the results of fetch- and duration-limited tests. The growth curves of JWA3G overlap with those of the SWAMP models, so that it is found

that the model gives valid results and each physical process fulfills the intended functions. The growth of wave energy in short fetch is a little greater than in the SWAMP models. In order to find the reason for this, some experiments were performed, in which the dissipation coefficient $C_b$ in $S_{ds}$ and the coupling coefficient $C$ in $S_{nl}$ are changed. The results of the experiments show that changing the coefficient $C_b$ has the effect of moving the growth curve parallel to the vertical axis, while changing the coefficient $C$ has the effect of increasing the gradient of the growth curve. Therefore the growth curve of the fetch-limited test gradually approaches those of the SWAMP results, if the coupling coefficient $C$ becomes larger. However the magnitude of the discrete interaction approximation also becomes larger in proportion to the magnitude of $C$, so that the magnitude of the nonlinear energy transfer is larger than the result of the exact calculation. The results indicate the limit of the discrete interaction approximation, so that it can be considered that a more highly-accurate scheme or exact scheme will be needed to improve the model.

The comparison between model results and Toba's 3/2 power law is shown in Figure 3.21. The model results agree well with the 3/2 power law except for the initial growth stage. So it is confirmed that the JWA3G model, in which the energy dissipation process is formulated so as to satisfy the 3/2 power law implicitly, gives the results as expected.

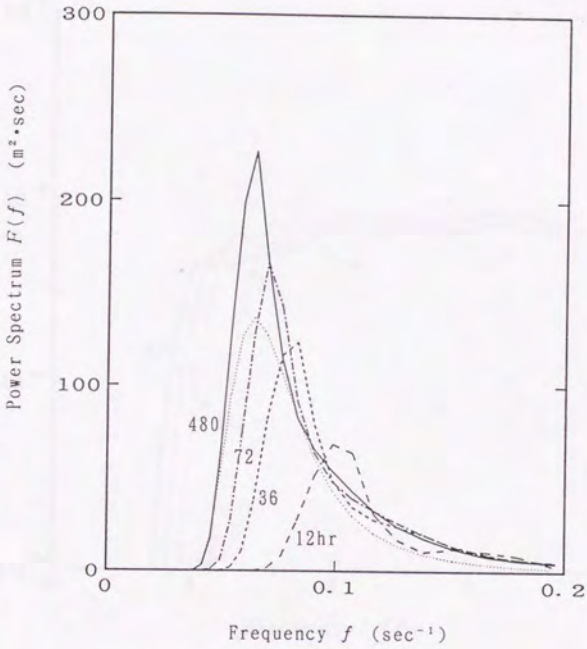


**Figure 3.13** Growth of the wind wave spectrum at the non-dimensional fetch $x^* = 7.1 \times 10^7$ under a stationary, homogeneous wind field with $u_{10} = 20$ m/s. The spectra at $t = 12$, 36 72 and 480 hours are shown. Dotted line corresponds to PM spectrum.

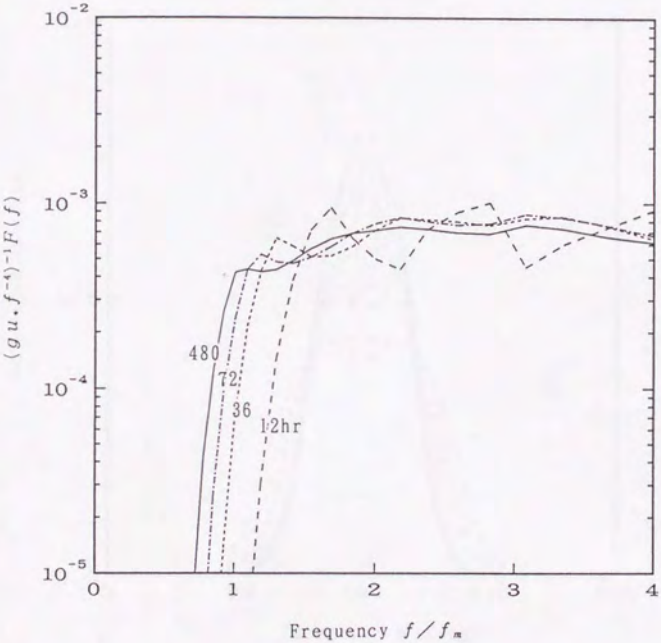


**Figure 3.14** Same as Figure 3.14, but with the spectrum multiplied by $gu.f^{-4}$. Frequency is normalized using the peak frequency $f_m$.

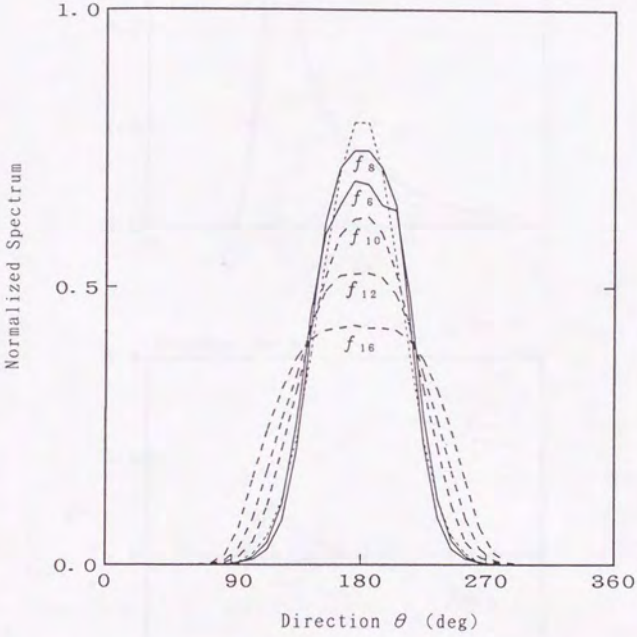


**Figure 3.15** Directional distribution of various wave components $f_n$ $(n = 6, 8, 10, 12, 16)$ at $t = 480$ hours. $f_8$ corresponds to the peak. Thin dashed line corresponds to $S = 8$ of Mitsuyasu's directional distribution function $\cos^{2S}\theta/2$.

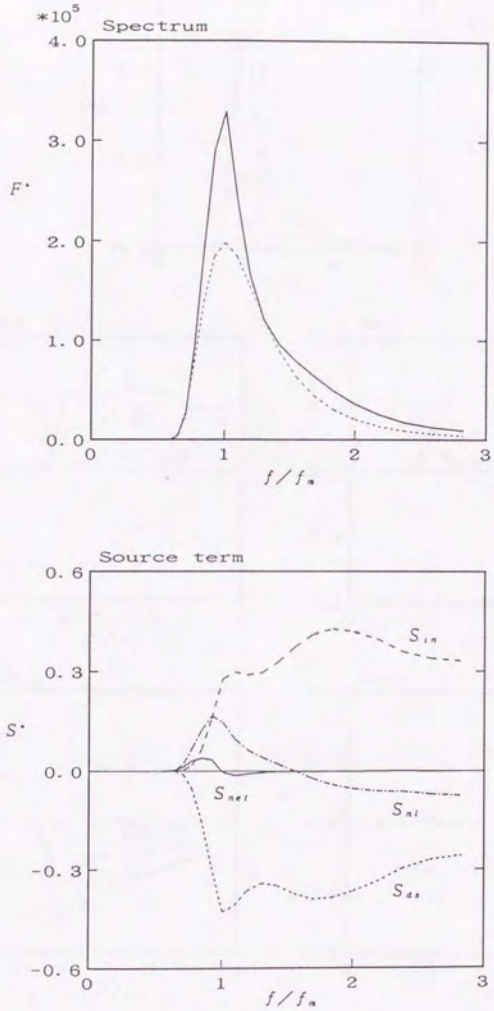


**Figure 3.16** Non-dimensionalized spectrum (solid line) at $t = 480$ hours with PM spectrum (dashed line) (upper) and energy source functions (lower). Frequency is normalized using the peak frequency $f_m$.

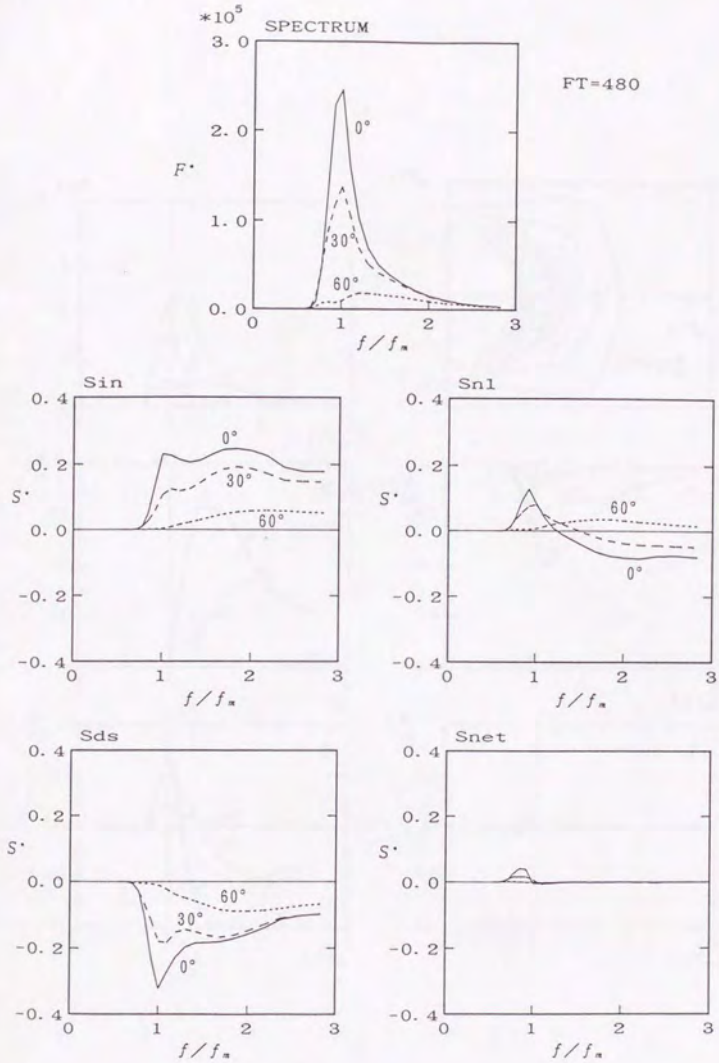


**Figure 3.17** Non-dimensionalized two-dimensional spectrum and source functions at various direction. Frequency is normalized using the peak frequency $f_m$.

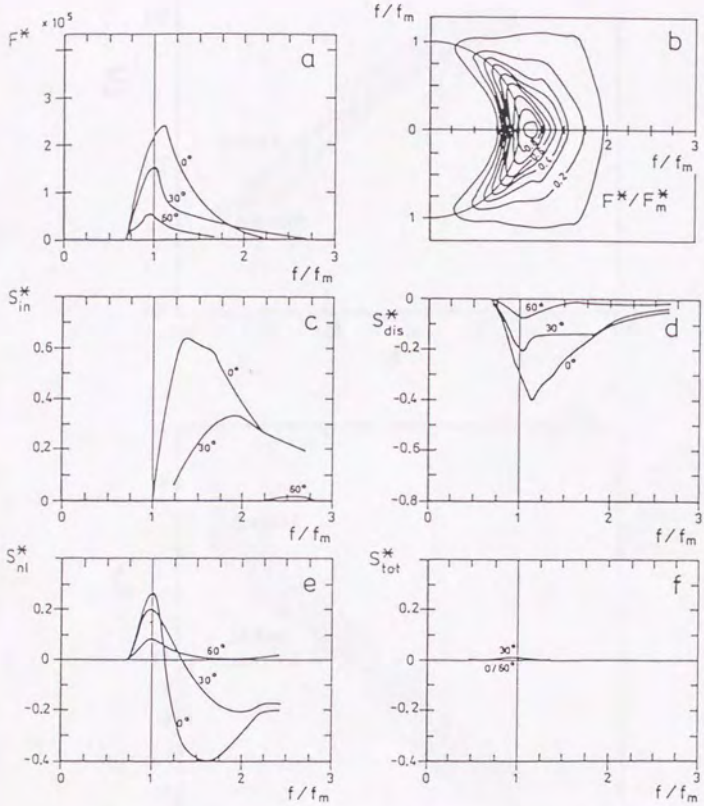


**Figure 3.18** Same as Figure 3.17, but from Komen *et al.* (1984). $S_{in}$ is based on Snyder *et al.* (1981), $S_{nl}$ is the exact calculation and $S_{ds}$ is determined by the numerical simulation. Frequency is normalized using the peak frequency $f_m$.

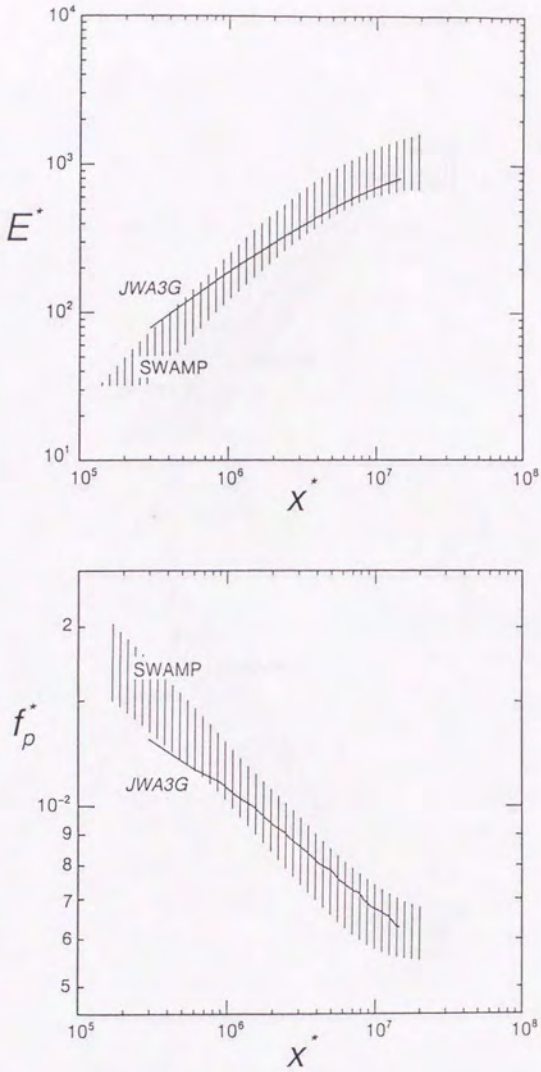


**Figure 3.19** Non-dimensional fetch-limited growth curve for the total wave energy (upper) and peak frequency (lower), compared with those of the SWAMP models (shaded area).

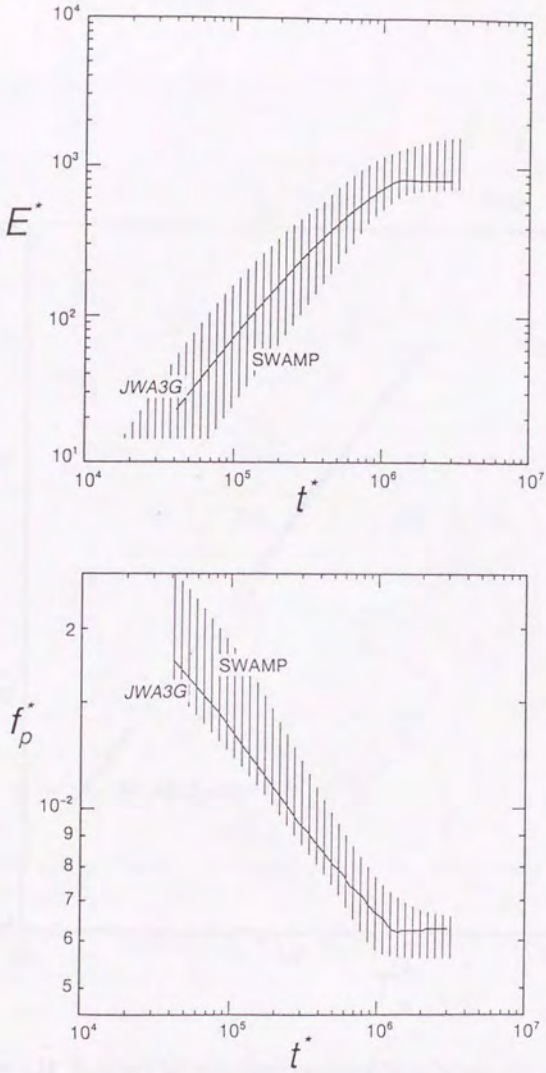


**Figure 3.20** Non-dimensional duration-limited growth curve for the total wave energy (upper) and the peak frequency (lower), compared with those of the SWAMP models (shaded area).

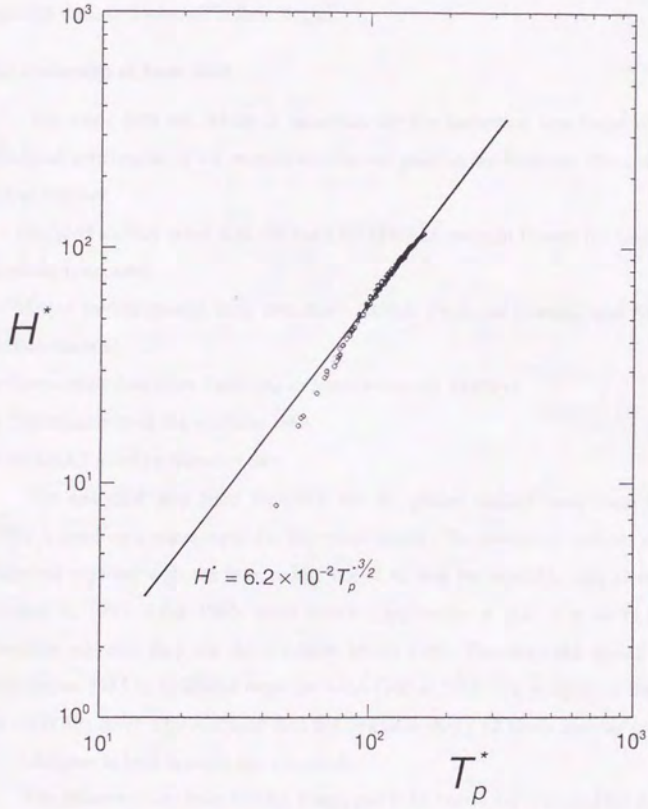


**Figure 3.21** Relations between nondimensional wave heights and periods in the JWA3G model (circle) for uniform wind, compared with Toba's 3/2 power law (solid line).

# 4. Verification of the JWA3G model

A global ocean wave hindcast for ten years, from 1980 to 1989, was performed using the JWA3G model. Verification of the model results, by comparing with buoy and satellite data, is discussed in this chapter.

## 4.1 Collection of basic data

The basic data set, which is necessary for the numerical simulation of the wave field and verification of the results, is collected prior to the hindcast. The collected data are as follows:

- Analyzed surface wind data set from ECMWF (European Centre for Medium-range Weather Forecasts)
- Marine environmental buoy data from NOAA (National Oceanic and Atmospheric Administration)
- Ocean buoy data from JMA (Japan Meteorological Agency)
- Statistical data of sea ice from JMA
- GEOSAT satellite altimeter data

The analyzed data from ECMWF for the global surface wind field (ECMWF, 1993) is used as a wind input for the wave model. The objective analysis model was improved together with the forecasting model, so that the available data elements were changed in 1985. After 1985, wind vector components $u$ and $v$ at 10 m height are available, whereas they are not available before 1985. Therefore the sea surface wind field before 1985 is estimated from the wind field at 1000 hPa in terms of the height at the 1000 hPa level. The analyzed data are available every 12 hours and the grid interval is 2.5 degrees in both latitude and longitude.

The observed data from NOAA buoys and JMA buoys are collected for the purpose of verification of the hindcast results. The grid size of 2.5 degrees (about 250 km) for wave calculation is so coarse that the accuracy of the wave calculation near the coast is insufficient. Therefore the data from buoys, which are located in the open sea, are collected. The locations of NOAA buoys are shown in Figures 4.1, 4.2 and 4.3 (NOAA, 1990). Although the shape of the NOAA buoys were the same discus buoy of 10 m in

diameter as the JMA buoys at the beginning of the observation, the shape was changed into a boat-shaped buoy, 6 m long and 3 m wide, except for Gulf coast buoys. NOAA buoy measurements are shown in Figure 4.1. The interval between the measurements is 1 hour. The parameters of wave height, momentum period and peak period are calculated from the wave spectrum, which is obtained from the spectrum of the accelerometer. Wave height is calculated from the 0th moment $m_0$ of the spectrum, while momentum period is calculated from the 1st moment $m_1$ of the spectrum (NOAA, 1994). The one-dimensional spectra are also available.

The locations of JMA buoys are shown in Figure 4.4 (JMA, 1990). Some observations by other buoys which are not shown in the figure, were operated temporarily; however, continuous buoy observations are available at the 4 stations shown in the figure. The position of buoy 21001 was moved from the initial position (Sanriku oki) to the south by about 2 degrees (Honshu toho oki) in 1987, but observation by buoy 21001 was halted in 1991. The shape of the JMA buoys is a discus buoy of 10 m in diameter. The measurements of wave height and period of JMA buoys are different from those of NOAA buoys. First, the displacement of buoy is calculated by twice integrating the voltage signal from the accelerometer. Then the averaged wave height is calculated from the displacement signal over 400 seconds, and the significant wave height is obtained by multiplying the averaged wave height by a factor 1.6. The factor 1.6 was derived from the statistical theory of Cartwright and Longuet-Higgins (1956). Wave period is calculated from the length of the time which is needed for counting 20 waves by detecting the zero-up-crossing points, where the displacement signal is changes from negative sign to positive sign. It is found that this method of measuring wave period has the problem that the zero-up-crossing points are mostly difficult to be detected, when the wave height is small. The observed elements of JMA buoys are shown in Table 4.2. The time interval of the observations is 3 hours; however, the interval time is automatically changed to 1 hour when the wind speed exceeds 35 knots.

The area for the wave calculation is confined within -70~70 degrees in latitude. In winter season, sea ice expands across 70 degree parallels of latitude. Since it is necessary to treat the area which is covered with sea ice with the same boundary

condition for land areas, sea ice data are collected. The distribution of sea ice is analyzed once a week at the Joint Ice Center of NOAA. Monthly mean distributions of sea ice (JMA, 1991a), which are made by using the weekly analyzed distribution, are collected in order to make a sea ice mask for the wave model. The sea ice mask with a 2.5 degrees interval is read off the figure of JMA (1991a).

The GEOSAT satellite was launched in March 1985 for the purpose of measuring the geoid of the earth. From November 1986, the ERM (Exact Repeat Mission) was started, in which the satellite returns to the same position with a period of about 17 days, and data from 62 cycles were obtained until September 1989 (NOAA, 1991). The radar altimeter measures the distance between the sensor and the sea surface. The measuring principle for wave height is schematically shown in Figure 4.5. The radar pulse emitted from the satellite is reflected first by the wave crests, and continuously reflected until the pulse passes through the wave troughs. So the change of the received power against the gate time is distorted as shown in Figure 4.6. The slope of the leading edge is directly affected by the wave height, namely, the inclination of the slope becomes smaller with increasing wave height. By using the relation, the significant wave height is calculated as an averaged value of 10 measurements during 1 second. The accuracy of the measurement is estimated as the greater value of either 0.5 m or 10 % of the wave height (Dobson *et al.*, 1987). In addition to the wave height parameter, the measurement of sea surface wind speed is available, however, its accuracy is found to be insufficient (Ebuchi *et al.*, 1992).

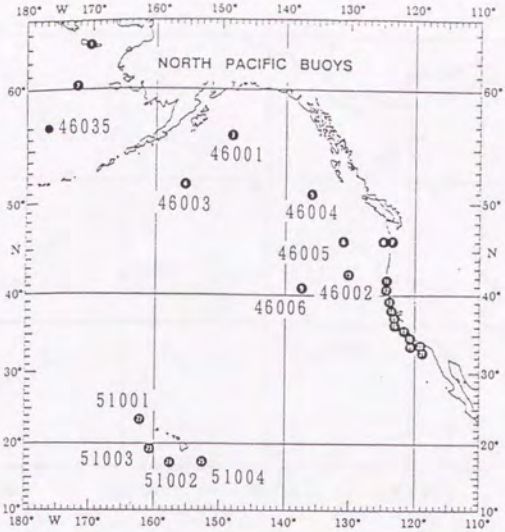


**Figure 4.1** Location of NOAA buoys (north Pacific and Hawaii). (from NOAA, 1990)

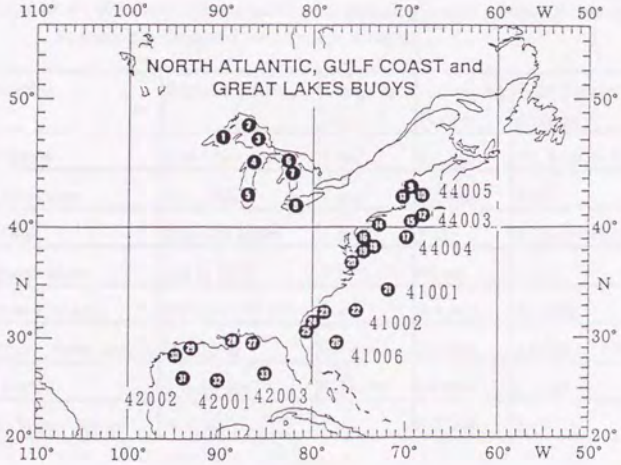


**Figure 4.2** Location of NOAA buoys (north Atlantic and Gulf Coast). (from NOAA, 1990)

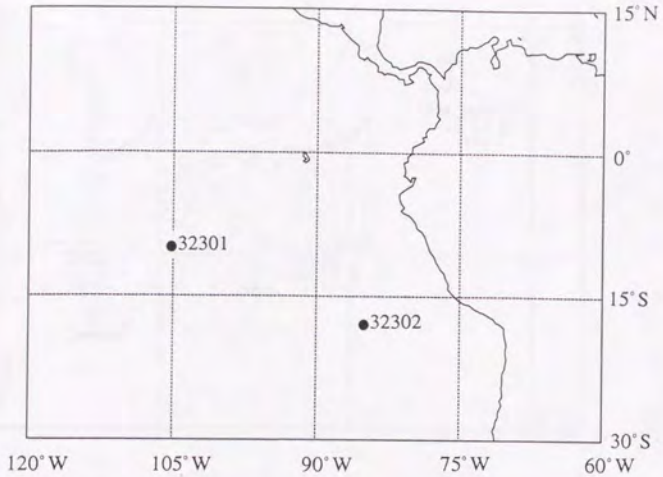


**Figure 4.3** Location of NOAA buoys (south Pacific).

**Table 4.1** NOAA buoy measurements with reporting ranges, sampling intervals, averaging periods and total system accuracy.

| Measurement | Reporting Range | Sampling Interval | Averaging Period | Total System Accuracy |
|---|---|---|---|---|
| Wind Speed | 0 to 120 knots | 1 sec | 8.5 min | ±1.9 knots or 10% |
| Wind Direction | 0 to 360° | 1 sec | 8.5 min | ±10° |
| Wind Gust | 0 to 160 knots | 1 sec | 5 sec | ±1.9 knots or 10% |
| Air Temperature | -40 to 50°C | 90 sec | 90 sec | ±1°C |
| Sea Level Pressure | 900 to 1100 hPa | 4 sec | 8.5 min | ±1 hPa |
| Significant Wave Height | 0 to 35 m | 0.39 sec | 20 min | ±0.2m or 5% |
| Wave Period | 3 to 30 sec | 0.39 sec | 20 min | ±1 sec |
| Surface Water Temp. | -7 to 41°C | 1 sec | 8.5 min | ±1°C |

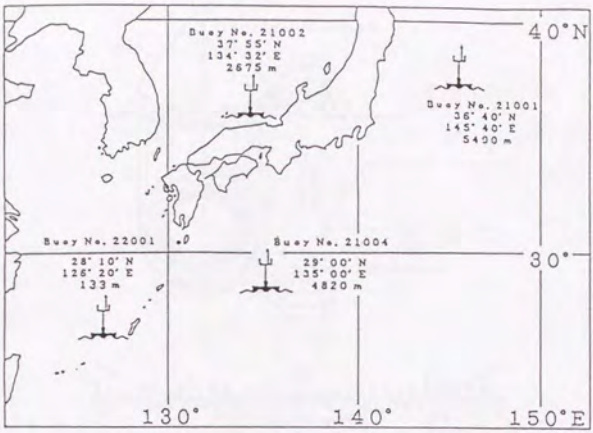


**Figure 4.4** Location of JMA buoys (from JMA, 1990).

**Table 4.2** JMA buoy measurements with measuring ranges.

| Measurement | Reporting Range |
|---|---|
| Wind Speed *) | 0 to 120 knots |
| Wind Direction | 0 to 360° |
| Air Temperature | -40 to 40°C |
| Wet-bulb Temperature | -10 to 40°C |
| Sea Level Pressure | 920 to 1040 hPa |
| Significant Wave Height | 0 to 20 m |
| Wave Period | 0 to 20 sec |
| Water Temperature at 1m depth | -10 to 40°C |
| Water Temperature at 50m depth | -10 to 40°C |
| Water Temperature at 100m depth | -10 to 40°C |
| Solar Radiation | 0 to 1.4kw/m$^2$ |

*) The height of anemometer is 7.5m.

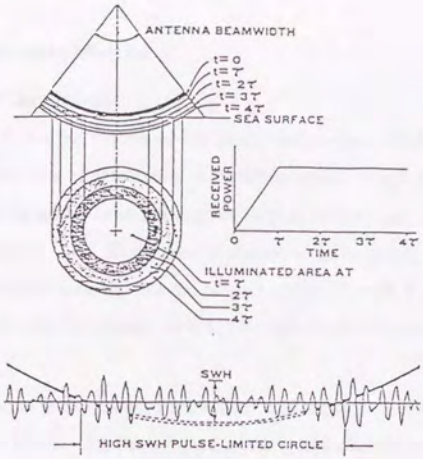


**Figure 4.5** Measurements of significant wave height (SWH) by radar altimeter (from Townsend *et al.*, 1981).

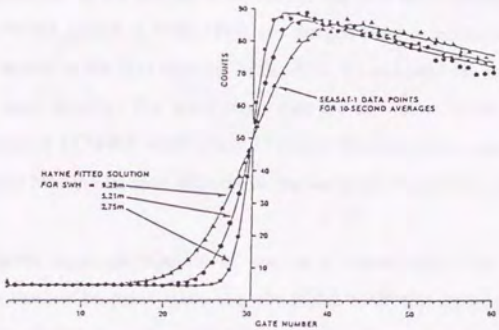


**Figure 4.6** Distortion of the received radar pulse. The slope of the leading edge is related to the significant wave height (from Townsend *et al.*, 1981).